ANTIOXIDANTS & REDOX SIGNALING
Volume 21, Number 16, 2014

DOI: 10.1089/ars.2014.5845

Discoveries

ORIGINAL RESEARCH COMMUNICATION

CD36 Upregulation Mediated by Intranasal LV-NRF2 Treatment Mitigates Hypoxia-Induced Progression of Alzheimer's-Like Pathogenesis

Chun-Yan Wang,[1–4,*] Zhan-You Wang,[1,2,*] Jing-Wei Xie,[1] Jian-Hui Cai,[5] Tao Wang,[1,2] Ye Xu,[3] Xu Wang,[6] and Li An[4]

Abstract

Aims: There is extensive evidence that oxidative stress induces cellular dysfunction in the brain and plays a critical role in Alzheimer's disease (AD) pathogenesis. Hypoxia increases factors involved in oxidative stress injury and contributes to the onset and progression of AD. Nuclear factor erythroid 2-related factor 2 (NRF2), a major component regulating antioxidant response, is attenuated in the AD brain. Importantly, NRF2 directly regulates the alternative first exons of CD36, an important participant in oxidative and inflammatory processes. To explore the effects of hypoxia-induced deterioration of AD-like pathogenesis and investigate the correlation between hypoxia-induced NRF2 signal alterations and CD36 expression, we examined the NRF2 signaling, CD36, and oxidative stress events in hypoxia-treated APPswe/PSEN1dE9 (APP/PS1) mice brain. ***Results:*** We observed that hypoxia treatment increased oxidative stress, exacerbated inflammation, and aggravated learning defects in aged APP/PS1 mice. Microglia from hypoxia-treated mice brain exhibited marked reduction in CD36 expression and inhibition of β-amyloid (Aβ) degradation. Accordingly, hypoxia treatment caused a decrease in transactivation of NRF2 target genes in the aging mouse brain. Intranasal administration with a lentiviral vector encoding human NRF2 increased CD36 expression, ameliorated the weak antioxidant response triggered by hypoxia, diminished Aβ deposition, and improved spatial memory defects. ***Innovation:*** In this study, we demonstrated for the first time that NRF2 intranasal treatment-induced increases of CD36 could enhance Aβ clearance in AD transgenic mouse. ***Conclusion:*** These results suggest that targeting NRF2-mediated CD36 expression might provide a beneficial intervention for cognitive impairment and oxidative stress in AD progression. *Antioxid. Redox Signal*. 21, 2208–2230.

Introduction

ALZHEIMER'S DISEASE (AD) is a common, age-associated neurodegenerative disease typified by progressive memory and cognitive function impairment. The main histological hallmarks observed in the AD brain include the extracellular accumulation of β-amyloid (Aβ) in neuritic plaques, neurofibrillary tangles, and neuronal loss (56). Hypoxia status resulting from hypertension, atherosclerosis, stroke, brain trauma, or diabetes mellitus is an important risk factor for AD (8, 52, 53, 65). Several studies have shown that individuals who suffered from neuronal hypoxia or ischemia were more susceptible to developing AD (16, 45). Hypoxia has been found not only to increase Aβ

[1]Key Laboratory of Medical Cell Biology of Ministry of Education of China, Department of Pathophysiology, China Medical University, Shenyang, China.
[2]College of Life and Health Sciences, Northeastern University, Shenyang, China.
[3]Medical Research Laboratory, Jilin Medical College, Jilin, China.
[4]Department of Nutrition and Food Hygiene, School of Public Health, China Medical University, Shenyang, China.
[5]Department of Surgery, Jilin Medical College, Jilin, China.
[6]Department of Histology and Embryology, Liaoning University of Traditional Chinese Medicine, Shenyang, China.
*These authors contributed equally to this work.

Innovation

In the present study, nuclear factor erythroid 2-related factor 2 (NRF2) expression can reverse some of the molecular aberrations associated with chronic hypoxic stress in an Alzheimer's disease (AD) model. We show for the first time that targeting NRF2-related CD36 levels may provide beneficial interventions for cognitive deficits and oxidative stress injury in AD progression, especially under chronic hypoxic conditions. Furthermore, our results support the feasibility of NRF2 gene therapy or small-molecule therapy in the treatment of AD.

generation and contribute to plaque formation, but also to worsen the memory deficit in an AD transgenic mouse model (68). Importantly, hypoxia has a significant impact on the loss of reactive oxygen species (ROS) homeostasis (26) and the stimulation of inflammatory gene expression (59). Increased ROS is also associated with aging and age-related degeneration (1). However, the molecular mechanisms that link hypoxia to AD pathogenesis are not well defined.

Glia, considered the primary immune effector cells for inflammation, is closely associated with AD (21, 48). CD36, a class B scavenger receptor expressed in microglia, is an important participant of oxidative, angiogenic, and inflammatory processes in the central nervous system (23, 30, 64). In the brain, CD36 is expressed in capillary endothelium (6), astrocytes (2), and microglial cells (13), and it is associated with the clearance of apoptotic neutrophils. It has been reported that CD36 mediates ROS production in response to Aβ fibrils (13). Furthermore, CD36 deficiency prevents neurovascular dysfunction in the Tg2576 mouse, a transgenic mice overexpressing the Swedish mutation of the amyloid precursor protein, and it is required for vascular oxidative stress both *in vivo* and *in vitro* (50). Aβ fibrillar-induced secretion of cytokines, chemokines, and ROS is significantly reduced in microglia and macrophages isolated from CD36 null mice. On the other hand, Hickman *et al.* observed that old transgenic AD mice had a two- to fivefold decrease in expression of the CD36 and Aβ-degrading enzymes of microglia compared with their wild-type (WT) littermate controls (28). It has been proposed that microglia phagocytosis is an Aβ-lowering mechanism of Aβ immunization in AD brain (3). Microglia exhibits age-associated decreases in the expression levels of CD36, and a fundamental decrease in Aβ phagocytosis ability is presented at an according age *in vitro* (24). Furthermore, macrophage and microglial recruitment with Aβ fibrillar treatment is reduced in CD36 null mice brain compared with WT mice (22). CD36-mediated microglia Aβ phagocytosis improved spatial memory performance in an AD transgenic model (76). The role of CD36 in the hypoxia-induced response in AD-related pathogenesis remains to be determined.

Nuclear factor erythroid 2-related factor 2 (NRF2) is one of the most regulated defense mechanisms guarding against oxidative stress (20, 37). NRF2 is important in the adaptive stress responses in preventing neurodegenerative diseases (10). Under physiological conditions, NRF2 binds to Kelch-like ECH associating protein 1 (Keap1) in the cytoplasm (47). On exposure to oxidative stress, NRF2 releases from Keap1, translocates to the nucleus, and binds to antioxidant-responsive elements (ARE) within the regulatory regions of genes encoding antioxidant enzymes and scavengers (17, 47). Importantly, nuclear NRF2 expression levels are significantly reduced in the hippocampus of AD *postmortem* brain (57). This lack of NRF2 renders astrocytes and cortical neurons susceptible to oxidative stress *in vitro* (37, 38). In contrast, small-molecule-induced activation of NRF2 provides sufficient protection against cerebral ischemia (69), and overexpression of NRF2 in astrocytes enhances the antioxidant function of co-cultured neurons (67). Further, NRF2 transduction results in memory improvement in an AD mouse model (34).

Interestingly, NRF2 can directly regulate gene expression of CD36 through its ARE (44). This has been demonstrated in a variety of tissue types. For example, NRF2 expression induces CD36 and other antioxidant stress genes in vascular smooth muscle cells within an atherosclerosis model. Likewise, nuclear accumulation of NRF2 in murine macrophages results in CD36 expression (32). In preadipocytes, the NRF2 signaling triggers CD36 overexpression by oxidized low-density lipoproteins (15). NRF2 activators enhance CD36 expression and CD36-mediated plasmodium phagocytosis *in vitro* (49). However, the role of NRF2 as a regulator of CD36 expression and its effect on the AD brain has not been elucidated.

To investigate the effects of hypoxia on CD36 expression and to identify the possible molecular mechanism by which NRF2 regulates CD36 gene expression in AD pathology, APPswe/PSEN1dE9 (APP/PS1) mice and age-matched WT C57BL/6 mice were subjected to chronic hypoxic conditions and assessed at 2, 6, and 12 months of age. We show that the decrease of CD36 triggered by hypoxia was age dependent and was accompanied by NRF2 down-regulation and microglial functional defects in the aging APP/PS1 mouse brain. Intranasal administration of a lentiviral vector expressing NRF2 induced CD36 expression and reduced hypoxia-mediated ROS production and neuroinflammatory events in the AD transgenic mouse brain.

Results

Hypoxia treatment aggravates learning deficits in aging APP/PS1 mice

Two-, six-, and 12-month-old male, APPswe/PSEN1dE9 (APP/PS1) double-transgenic (Tg) mice and age-matched, male, WT C57BL/6 mice received hypoxia treatment (Hypo) once daily for 2 months, after which behavioral testing was performed. Morris water maze (MWM) and Y-maze tests were used to assess the effects of hypoxia treatment on learning and memory. As illustrated in Figure 1, mice were tested for 8 consecutive days using the MWM trial and three-arm radial Y-maze.

In the MWM trial, the mean swimming velocity, escape latency to the platform, the path length of each trial, and the passing times that the mouse crossed the invisible platform were recorded. All mice of different genotypes were able to swim in a coordinated way. During the first 2 days of MWM testing, WT and Tg mice exhibited comparable performance in the escape latency in visible platform tests ($p > 0.05$; Fig. 1A). Some motivational or motor defects were observed in

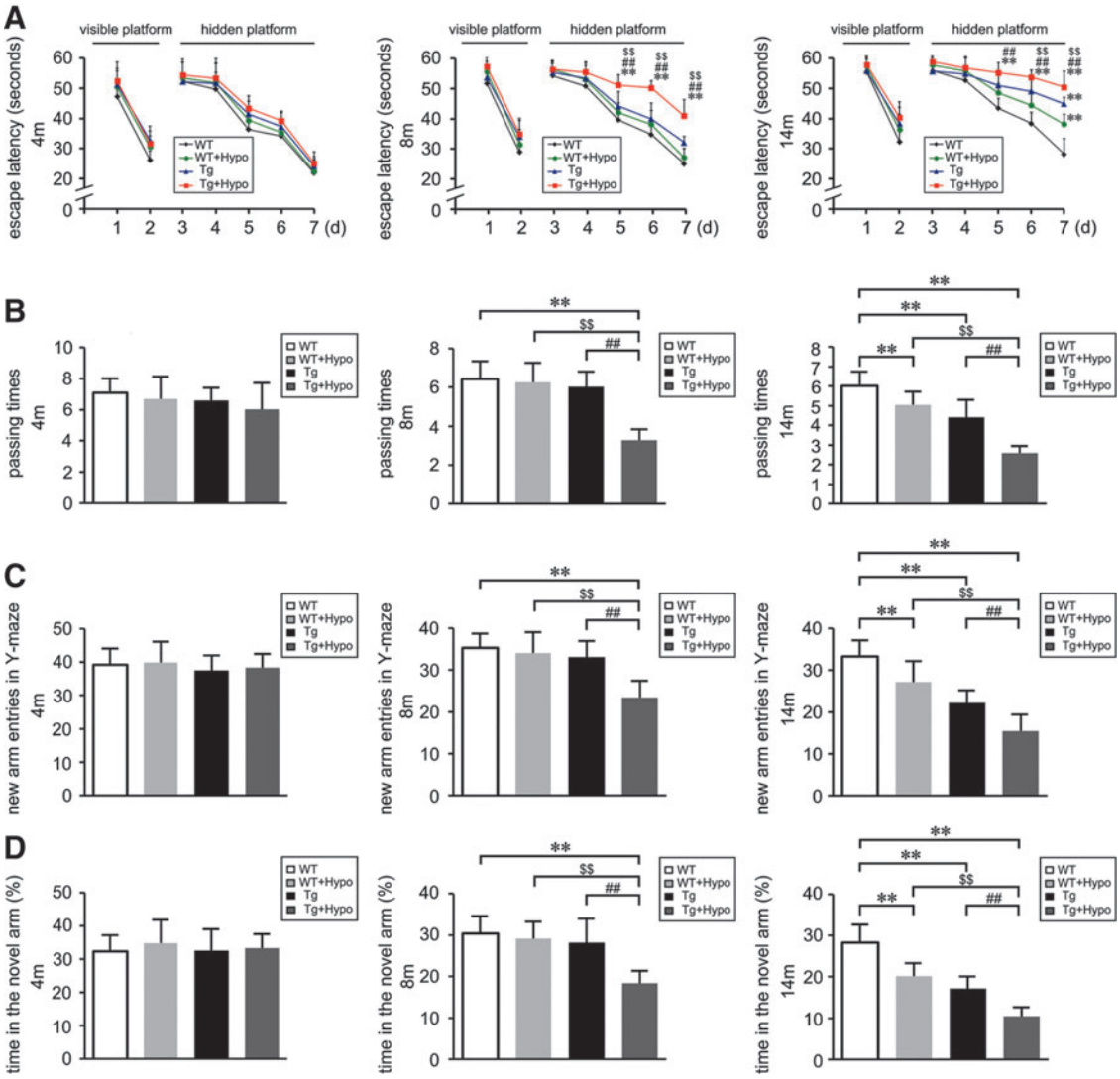

FIG. 1. Hypoxia treatment impairs the spatial learning and memory in the aging APP/PS1 mice. Two-, six-, and 12-month-old double APP/PS1 transgenic (Tg) and age-matched wild-type (WT) C57BL/6 mice were treated with hypoxia intervention (Tg + Hypo, WT + Hypo) or control conditions (Tg, WT) for 2 months. **(A, B)** The Morris water maze (MWM) was performed at varying ages after hypoxia intervention. The procedure consisted of 2 days of visible platform tests, 5 days of hidden platform tests, and 1 day of probe trials. **(C, D)** Y-maze test for spatial learning and memory showed the novel arm entries and percentage of time spent in the novel arm during the trial of the mice. $^{**}p < 0.01$ *versus* WT group, $^{\#\#}p < 0.01$ *versus* Tg group, $^{\$\$}p < 0.01$ *versus* WT + Hypo group by repeated-measures analyses of variance (ANOVA) ($n = 8$ in each group). Data are represented as mean ± standard error of the mean values (SEM).

both WT and Tg mice under hypoxia treatment with a trend toward a decrease in swimming speed at the age of 14 months (data not shown). In the next 5 days of hidden platform tests, Tg + Hypo mice showed a longer escape latency compared with age-matched WT, Tg, and WT + Hypo mice ($p < 0.01$; Fig. 1A) at 8 and 14 months of age. In the probe trial on the last day, the passing times that Tg + Hypo mice crossed the center of the northwest quadrant were significantly less compared with age-matched 8- and 14-month-old WT and Tg mice ($p < 0.01$; Fig. 1B). Furthermore, at 14 months of age, hypoxia treatment induced a deficit in the probe trial of WT + Hypo mice compared with age-matched WT mice ($p < 0.01$; Fig. 1B). The results indicate that genotypes associated with familial AD lead a learning deficit in aging APP/PS1 mice. Hypoxia treatment aggravates the effects. The impairment of spatial memory induced by hypoxia is prominent in the aged WT mice

Compared with age-matched WT and Tg mice, hypoxia-treated Tg mice exhibited worse recognition in the Y-maze novel arm at 8 and 14 months of age ($p < 0.01$; Fig. 1C, D). In contrast, at 14 months old, the new arm entries (Fig. 1C) and percentage of time spent in the novel arm (Fig. 1D) of the WT + Hypo mice was less compared with control WT mice ($p < 0.01$).

The loss of synaptic markers is related with the disease progression and cognitive decline in AD (61). Accordingly, we examined hypoxia-induced protein expression changes of synaptic markers in the mouse brain by Western blot using anti-

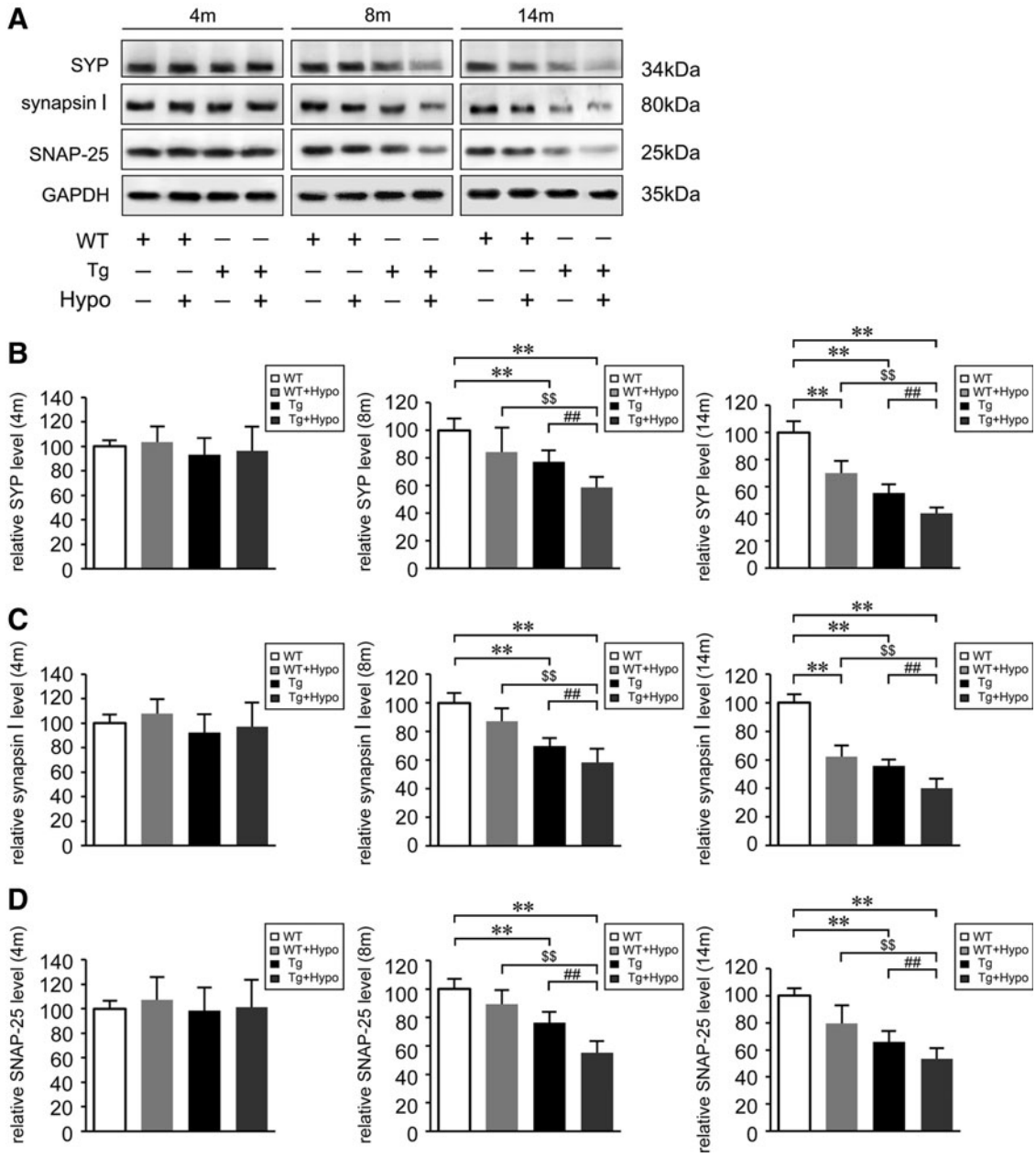

FIG. 2. Hypoxia reduces synaptic markers protein levels in the aging APP/PS1 mice. (A) Representative Western blot images of synaptic markers, detected with anti-synaptophysin (SYP), anti-synapsin I, and anti-synaptosomal-associated protein 25-kDa (SNAP-25), and normalized to GAPDH in the brains of APP/PS1 transgenic (APP/PS1) mice and age-matched WT C57BL/6 mice. **(B–D)** Quantification indicates the levels of SYP, synapsin I, and SNAP-25 in the mice brain. $^{**}p<0.01$ *versus* WT group, $^{\#\#}p<0.01$ *versus* Tg group, and $^{\$\$}p<0.01$ *versus* WT + Hypo group by two-way ANOVA, $n=6$–8 in each group. Values represent the mean ± SEM.

synaptophysin (SYP), anti-synapsin I, and anti-synaptosomal-associated protein 25-kDa (SNAP-25) antibodies. As shown in Figure 2, under hypoxia treatment, the expression of SYP (Fig. 2A, B), synapsin I (Fig. 2A, C), and SNAP-25 (Fig. 2A, D) was significantly reduced in hypoxia-treated Tg mice compared with age-matched WT and Tg control mice at 8 and 14 months of age ($p<0.01$). WT mice subjected to hypoxic conditions also displayed a decrease in the protein levels of SYP (Fig. 2A, B) and synapsin I (Fig. 2A, C) in the 14-month-old mouse brain ($p<0.01$).

Hypoxia treatment increases oxidative stress and exacerbates inflammation in the APP/PS1 and WT aging mouse brain

Considering the critical role of oxidative stress in AD-related pathogenesis, we assayed ROS levels in the mouse brain using the CM-H_2DCFDA assay. As illustrated in Figure 3, chronic hypoxia treatment induced higher ROS levels in the APP/PS1 mouse brain compared with age-matched WT and Tg control brains at 8 and 14 months age ($p<0.01$; Fig. 3A).

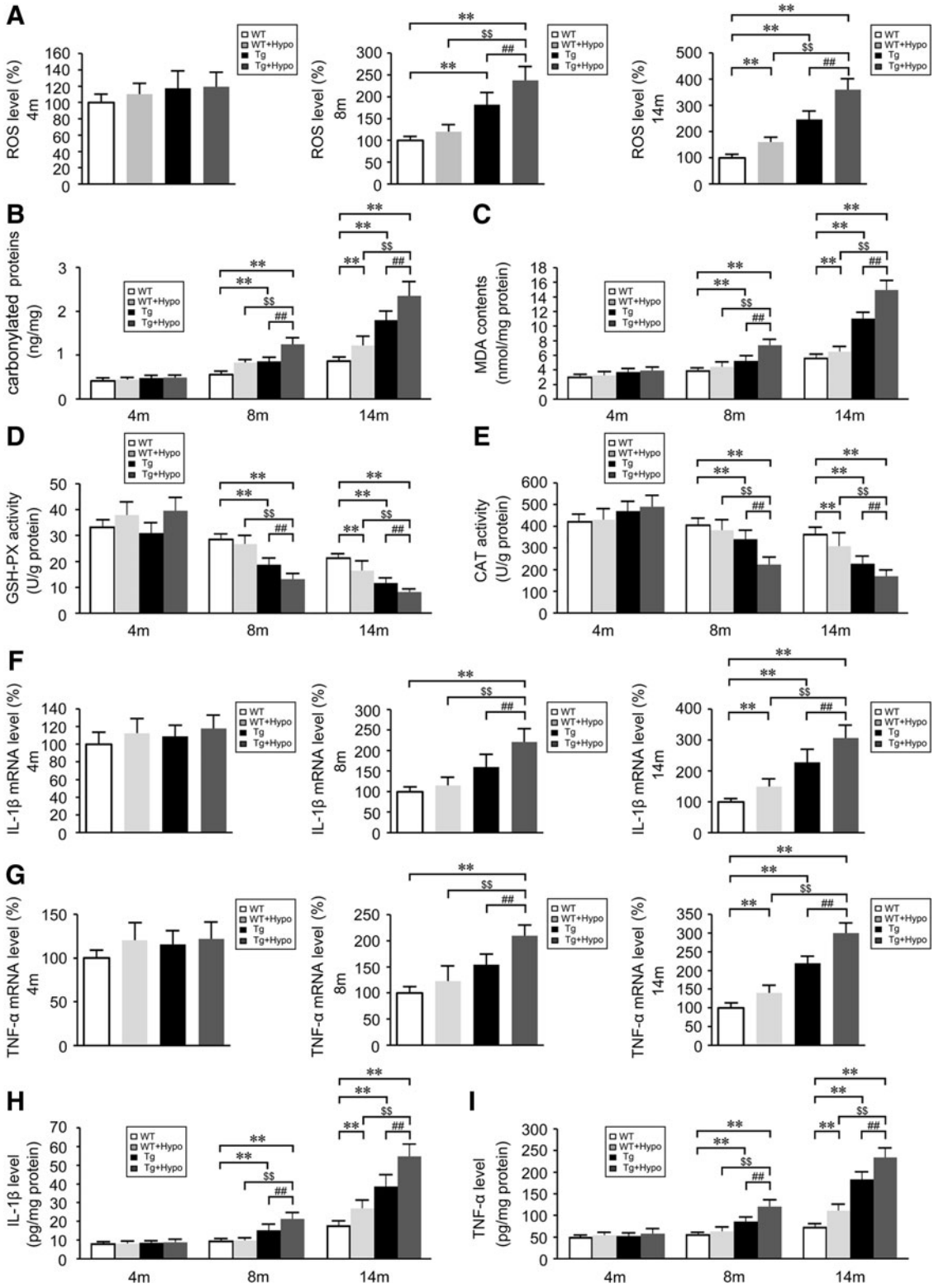

FIG. 3. Hypoxia increases oxidative stress and inflammatory events in the brain of APP/PS1 and aging WT mice. Reactive oxygen species (ROS) levels **(A)**, carbonyl proteins **(B)**, and malondialdehyde (MDA) contents **(C)** in the brains of APP/PS1 transgenic (Tg) and aging WT mice. **(D, E)** Activities of antioxidant enzymes, glutathione peroxidase (GSH-PX), and catalase (CAT). Relative mRNA expression of interleukin (IL)-1β **(F)** and tumor necrosis factor-α (TNFα) **(G)** normalized to β-actin in CD11b$^+$ cells from Tg and age-matched WT brains. ELISA analyses show the levels of IL-1β **(H)** and TNFα **(I)**. $^{**}p < 0.01$ *versus* WT group, $^{\#\#}p < 0.01$ *versus* Tg group, $^{\$\$}p < 0.01$ *versus* WT + Hypo group by repeated-measures ANOVA, $n = 6$–8 in each group. Values represent the mean ± SEM.

A similar effect of hypoxia was observed with ROS production in WT mice at 14 months of age as well ($p < 0.01$; Fig. 3A).

We then assessed the carbonylated proteins and the contents of the lipid peroxidation product, malondialdehyde (MDA). Hypoxia treatment increased the accumulation of carbonylated proteins and MDA production in the 8- and 14-month-old Tg mouse brain ($p < 0.01$; Fig. 3B, C). The significant differences in the levels of carbonylated proteins and MDA between WT and WT + Hypo group were shown at 14 months age ($p < 0.01$; Fig. 3B, C). We then asked whether the accumulation was associated with alterations of antioxidant enzyme activity. As shown in Figure 3D and E, the activities of glutathione peroxidase (GSH-PX) and catalase (CAT) in the Tg mice brain were reduced compared with age-matched WT mice at 8 and 14 months of age ($p < 0.01$). Hypoxia exacerbated the down-regulation of GSH-PX and CAT activities in the Tg mouse brain at 8- and 14 months of age (Tg + Hypo) compared with age-matched WT and Tg control groups ($p < 0.01$). In contrast, the significant decrease of GSH-PX and CAT activities in the WT mouse brain triggered by hypoxia treatment was observed by 14-month-old mice ($p < 0.01$; Fig. 3D, E).

To evaluate the inflammatory response induced by hypoxia in the mouse brain, the expression of the pro-inflammatory cytokines interleukin-1β (IL-1β) and tumor necrosis factor-α (TNFα) were assayed by real-time PCR and ELISA. Compared with age-matched control WT and Tg brains, hypoxia stimulation resulted in a marked increase of IL-1β and TNFα mRNA levels in $CD11b^+$ cells isolated from Tg brains (Tg + Hypo) at 8 and 14 months of age ($p < 0.01$; Fig. 3F, G). The levels of IL-1β and TNFα mRNA were increased in the hypoxia-treated WT mice brain at 14 months of age ($p < 0.01$; Fig. 3F, G). Likewise, ELISA analysis showed that hypoxia treatment significantly enhanced the production of IL-1β ($p < 0.01$; Fig. 3H) and TNFα ($p < 0.01$; Fig. 3I) in the cortices of Tg mouse brains (Tg + Hypo) compared with age-matched WT and Tg control brains. Similar effects of hypoxia on IL-1β and TNFα levels in the WT mice brain were observed at 14 months of age ($p < 0.01$; Fig. 3H, I). Hypoxia-inducible factor 1α (HIF1α), a master regulator of the cellular response to hypoxia, is stabilized and activated by hypoxia (62). Under hypoxia stimulus, HIF-mediated gene expression can affect ROS generation (26). Low levels of free radicals increase HIF1α expression and induce neuroprotection (12). In our present study, an instant transient increase of HIF1α protein expression accompanied by an increase in its mRNA expression were observed in the mice brain in initial hypoxia treatment in the mice brain of both genotypes (Supplementary Fig. S1; Supplementary Data are available online at www.liebertpub.com/ars); whereas the levels of HIF1α protein and mRNA expressions were reduced in hypoxia-treated Tg mice brain with 2 months of hypoxia intervention (Supplementary Fig. S1). The alterations in HIF1α levels after long-term hypoxia administration might be a chronic response (54). It has been shown that the HIF levels are reduced in AD patients (43). Schubert *et al.* reported that Aβ-dependent glial activation results in a decrease in HIF1α expression (60). It is likely that the hypoxia treatment might increase Aβ accumulation, which conversely inhibits HIF1α in the AD mice brain.

Hypoxia increases soluble Aβ levels and worsens Aβ deposition in the APP/PS1 mouse brain

Cortical levels of mouse Aβ1-40 and Aβ1-42, and human Aβ1-40 and Aβ1-42 in mouse brains were determined by sandwich ELISA. As shown in Figure 4, there was no significant difference in the levels of soluble mouse Aβ1-40 and Aβ1-42 among groups although there was a trend toward an increase in the hypoxia-treated group compared with the control group ($p > 0.05$; Fig. 4A, B). The levels of human soluble Aβ1-40 (Fig. 4C) and Aβ1-42 (Fig. 4D) in hypoxia-treated Tg mouse brains were significantly increased compared with control Tg mice at 8 and 14 months of age ($p < 0.01$), and all the effects of hypoxia on human insoluble Aβ1-40 (Fig. 4E) and insoluble Aβ1-42 (Fig. 4F) contents were increased as well. The ratio of human soluble Aβ42 to Aβ40 in the brain of hypoxia-treated Tg mice was higher than the Tg group without hypoxia treatment by 8 months of age ($p < 0.01$, Fig. 4G). Typically, the elevation of human insoluble Aβ42/40 ratios was significantly prominent in the hypoxia-treated Tg group compared with untreated Tg mice at 8- and 14 months of age ($p < 0.01$, Fig. 4H). To further characterize Aβ deposition, immunostaining with anti-Aβ antibody was used to detect Aβ plaques. As shown in Figure 5, at 4 months of age, Aβ plaques were not observed in Tg mouse brain sections; while Tg + Hypo mouse brain tissues had sparse, but detectable Aβ deposits. Increasing Aβ plaque formation from Tg mouse brain tissues was prominent at 8 and 14 months of age. Hypoxia treatment enhanced the Aβ plaque deposition in Tg mice brain. Quantification indicated that the Aβ plaque number and immunoreactive areas in Tg mouse brain of hypoxia-treated groups (Tg + Hypo) were significantly increased in the cortex and hippocampus compared with the age-matched Tg group at 8- ($p < 0.01$; Figs. 4I and 5) and 14 months of age ($p < 0.01$; Figs. 4J and 5).

Microglia exhibit marked reduction in the expression of CD36 and Aβ-degrading enzymes with hypoxia treatment in the aging mouse brain

Microglia, the major phagocytic cell of the brain, may mediate clearance of Aβ. Microglia express receptors such as CD36 (21), a class B scavenger receptor, and secrete Aβ-degrading enzymes to promote the clearance and phagocytosis of Aβ (39). To investigate whether hypoxia-induced Aβ deposition in the APP/PS1 mouse brain was associated with deficient phagocytosis and degradation of Aβ, the level of the messengers RNA for Aβ-binding receptor, CD36, and Aβ-degrading enzymes of microglia in the mouse brain were assessed. We isolated the microglia with cell markers for microglia, mouse anti-CD11b-coated microbeads. Real-time PCR analysis of CD36 from $CD11b^+$ cells isolated from mouse brains indicated that there was an increase in the mRNA levels of CD36 in both the WT and Tg groups under hypoxic conditions at 4 months of age ($p < 0.01$; Fig. 6A). However, the expression of CD36 was significantly reduced in $CD11b^+$ cells from hypoxia-treated Tg mice compared with age-matched WT and Tg controls by 8 and 14 months of age ($p < 0.01$; Fig. 6A). In addition, hypoxia-induced reduction of CD36 expression was observed in 14-month-old WT + Hypo group compared with the age-matched WT controls ($p < 0.01$; Fig. 6A).

To determine the expression levels of Aβ-degrading enzymes under hypoxic conditions, real-time PCR was carried

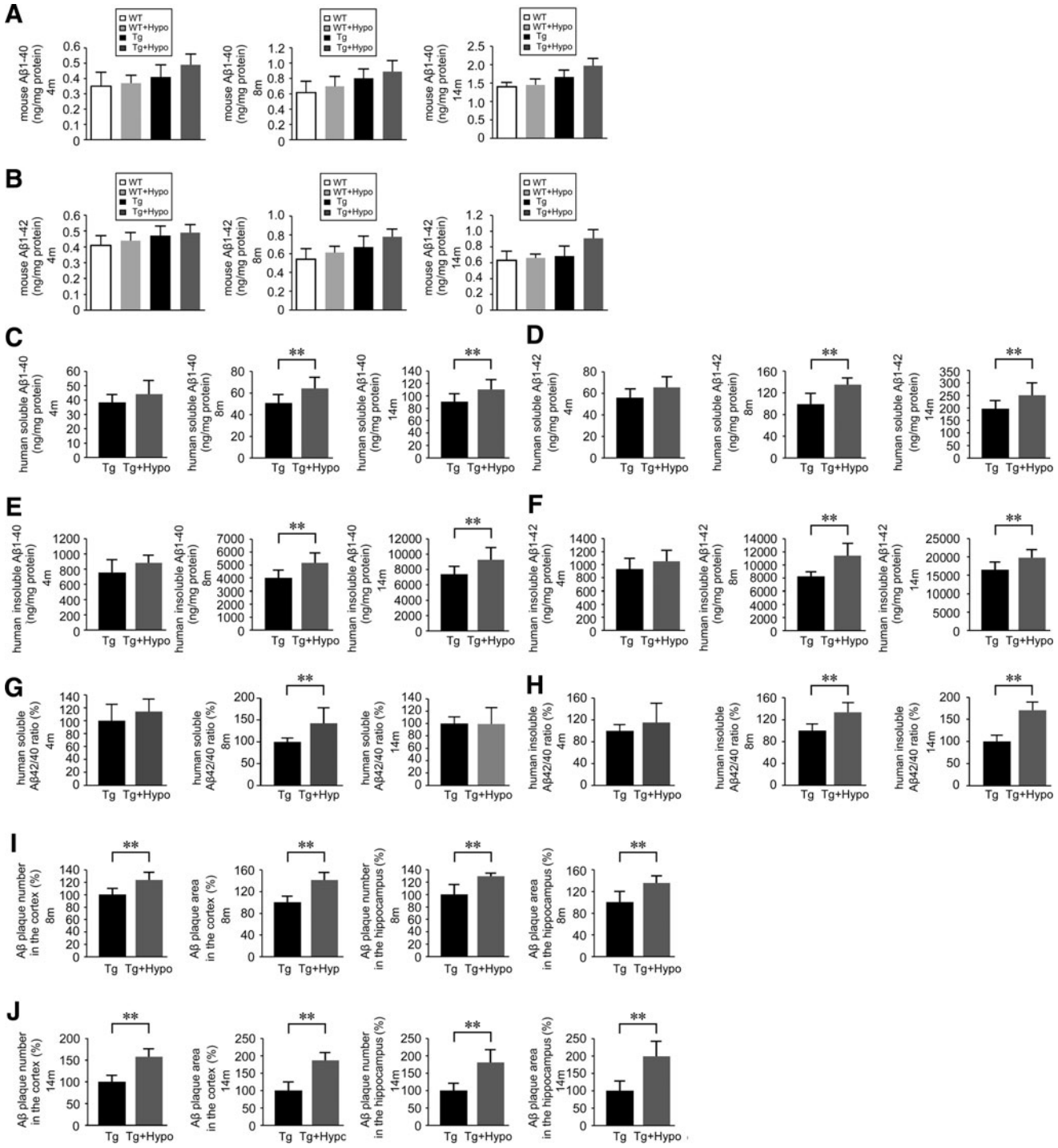

FIG. 4. Hypoxia treatment markedly increases *β*-amyloid burden in the aging APP/PS1 mouse brain. Levels of mouse soluble Aβ1-40 **(A)** and Aβ1-42 **(B)** were determined by ELISA in the APP/PS1 transgenic (Tg) and age-matched WT C57BL/6 mouse brain. Two-way ANOVA were performed, $n = 6$–8 in each group. Data are represented as mean ± SEM. **(C–F)** Quantification shows human soluble Aβ1-40, Aβ1-42, insoluble Aβ1-40, and Aβ1-42 contents in the Tg mouse brain. **(G)** The ratio of human soluble Aβ42 to Aβ40 in the Tg mice brain. **(H)** Human insoluble Aβ42/40 peptide ratios in the brain of Tg mice. **(I, J)** Quantification shows the Aβ plaque number and area in the cortex and hippocampus of the Tg mouse brain. Five brain sections per mouse were examined. $^{**}p < 0.01$ *versus* Tg group by Student's *t*-test, $n = 6$–8 in each group. Data are represented as mean ± SEM.

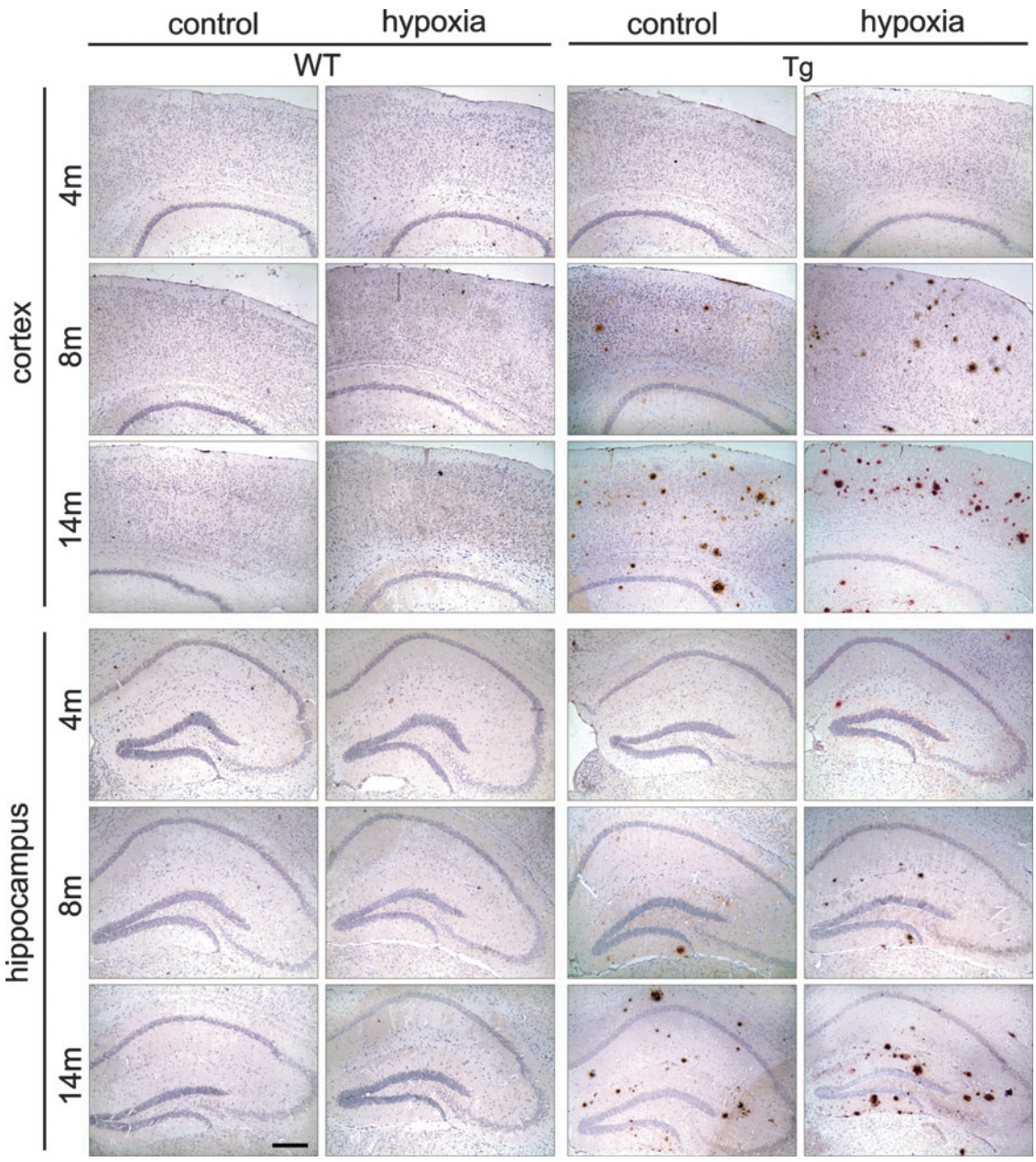

FIG. 5. Representative images of Aβ plaques in APP/PS1 and age-matched C57BL/6 mice brain. Aβ plaques were examined with anti-Aβ antibody. Aβ-positive plaques were significantly detectable in the cortex and hippocampus of APP/PS1 transgenic (Tg) mice brain at 8- and 14 months of age, especially in the group that underwent hypoxia treatment. There was no Aβ-positive plaque in the age-matched WT C57BL/6 mice brain. Scale Bar = 200 μm.

out to measure the mRNA levels of insulin degradation enzyme (IDE), neprilysin (NEP), and matrix metalloproteinase-9 (MMP-9) in $CD11b^+$ cells isolated from APP/PS1 mice and age-matched WT mouse brains. As shown in Figure 6B, hypoxia treatment significantly reduced the IDE mRNA levels in the brains of Tg mice (Tg + Hypo) compared with age-matched WT and Tg controls ($p < 0.01$; Fig. 6B) at 8- and 14 months in the Tg mouse brain ($p < 0.01$; Fig. 6B). Hypoxia treatment caused a decrease in NEP and MMP-9 ($p < 0.01$; Fig. 6C, D) mRNA expression levels of the Tg mouse brain (Tg + Hypo) compared with the age-matched WT ($p < 0.01$; Fig. 6C, D) and Tg control group ($p < 0.01$; Fig. 6C, D) at 14 months of age. Furthermore, the expression of IDE and NEP mRNA levels in WT + Hypo mice was markedly reduced compared with the WT control groups ($p < 0.01$; Fig. 6B, C) in $CD11b^+$ cells in the 14-month-old mouse brain.

Hypoxia results in a pronounced attenuation of the NRF2-ARE pathway in the brain of aged APP/PS1 and WT mice

Binding of NRF2 to the ARE switches on an endogenous defense system against oxidative stress (33, 74). The lack of NRF2 renders astrocytes and cortical neurons increasingly susceptible to oxidative stress *in vitro* (37, 38). In the present

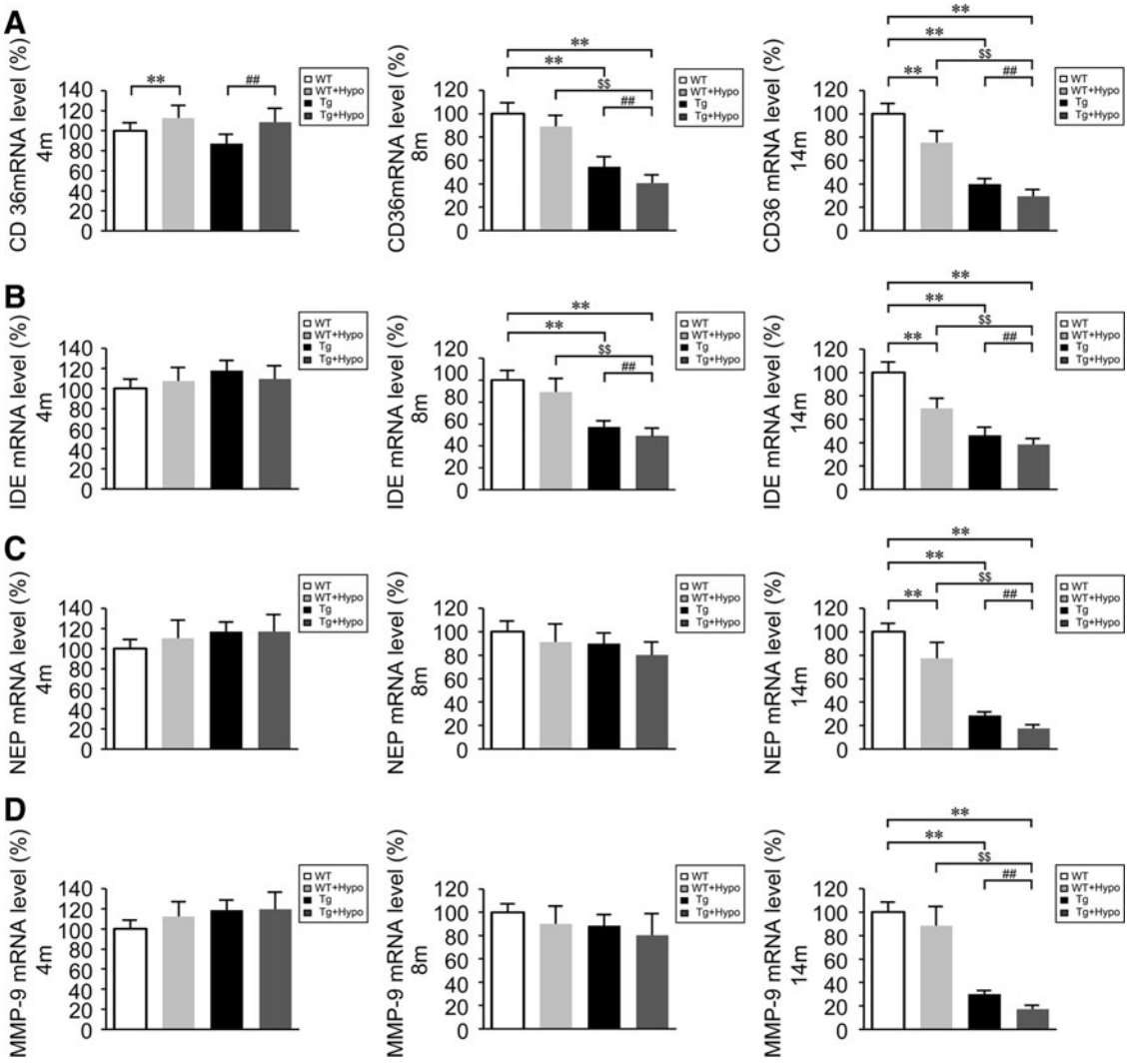

FIG. 6. Hypoxia significantly reduces the expression of CD36 and Aβ-degrading enzymes in the aged mouse brain. **(A)** Relative expression of CD36 mRNA was normalized to β-actin in CD11b$^+$ cells from the brains of APP/PS1 transgenic (Tg) and age-matched WT C57BL/6 mice. **(B–D)** The mRNA expression of Aβ-degrading enzymes, insulin degradation enzyme (IDE), neprilysin (NEP), and matrix metalloproteinase-9 (MMP-9) in CD11b$^+$ cells from Tg and WT brains was assessed by real-time PCR. $^{**}p < 0.01$ *versus* WT group, $^{\#\#}p < 0.01$ *versus* Tg group, and $^{\$\$}p < 0.01$ *versus* WT + Hypo group by two-way ANOVA, $n = 6$–8 in each group. Values represent the mean ± SEM.

study, we examined whether chronic hypoxia induced oxidative stress and neuroinflammation in the AD mouse brain through the NRF2-ARE pathway. Western blot assays showed that the levels of nuclear NRF2 were increased in hypoxia-treated Tg mouse brain tissues compared with the age-matched Tg group without hypoxia administration at 4 months of age ($p < 0.01$; Fig. 7A, C). The nuclear NRF2 levels in the hypoxia-treated WT mouse brain were also higher than WT controls at 4 months of age ($p < 0.01$; Fig. 7A, C). However, by 8 and 14 months of age, the nuclear NRF2 levels in the Tg + Hypo mouse brain were reduced compared with age-matched WT ($p < 0.01$; Fig. 7A, C) and Tg controls ($p < 0.01$; Fig. 7A, C), and the alterations of cytosolic NRF2 levels were in the hypoxia-treated Tg group compared with WT ($p < 0.01$; Fig. 7A, B) and Tg controls ($p < 0.01$; Fig. 7A, B). Meanwhile, hypoxia treatment caused a significant attenuation of NRF2 signal in WT mice at 8 and 14 months of age ($p < 0.01$; Fig. 7A–C). Assessment of NRF2 DNA-binding activity (Fig. 7D) using an ELISA kit and analysis of NRF2 mRNA levels by real-time PCR (Fig. 7E) confirmed earlier results. These data indicate that the NRF2 signal might be activated under hypoxia stimulation in the 4-month-old WT and Tg mice brain; while NRF2 levels are reduced with hypoxia treatment in the aged mice brain, especially in the APP/PS1 transgenic mice.

We then examined the protein expression levels of the NRF2-ARE-driven antioxidants heme oxygenase-1 (HO-1), nicotinamide adenine dinucleotide phosphate quinone oxidorreductase-1 (NQO1), catalytic subunits of γ-glutamyl cysteine ligase (γGCL-C), and modulatory subunits of γ-glutamyl cysteine ligase (γGCL-M) by Western blot. As shown in Figure 8, at 4 months of age, there was no difference in the expression of NQO1, γGCL-C, and γGCL-M ($p > 0.05$; Fig. 8A, C–E) in the WT and Tg mice brain except that HO-1 protein levels were slightly increase in the hypoxia-treated mice compared with the control groups ($p < 0.01$; Fig. 8A,

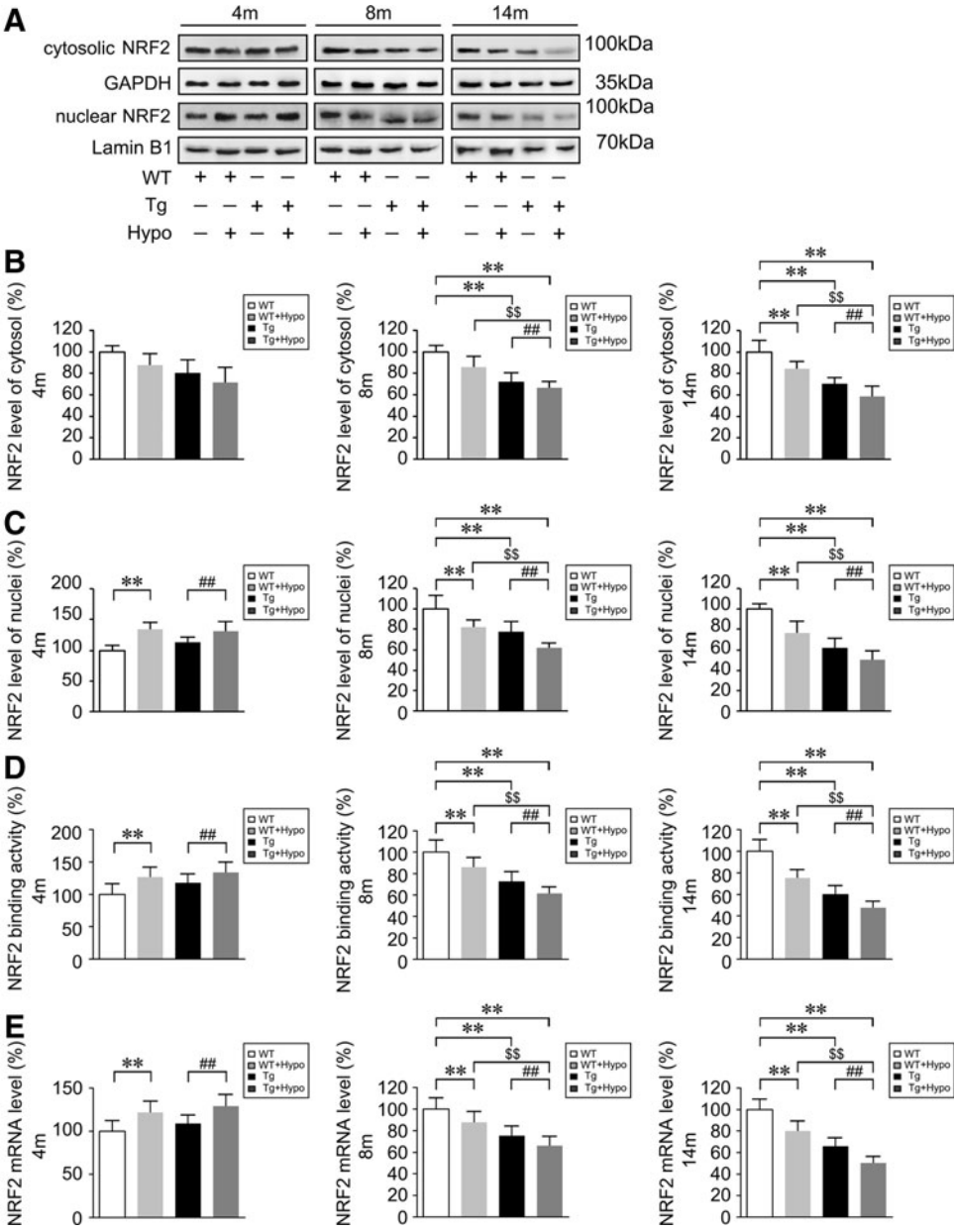

FIG. 7. Nrf2 levels are altered and significantly reduced under hypoxic conditions in the aging mouse brain. (A–C) Nuclear factor erythroid 2-related factor 2 (NRF2) in the cytosolic and nuclear fractions from APP/PS1 transgenic (Tg) and age-matched WT C57BL/6 mice brain tissues were analyzed with anti-NRF2 antibody (Abcam). As loading controls, the levels of GAPDH and Lamin B1 were determined to ensure equal amounts of total and nuclear protein, respectively. **(D)** NRF2 DNA-binding activity examined by ELISA. **(E)** Relative expression NRF2 nuclear mRNA levels normalized to the levels of β-actin. $^{**}p<0.01$ *versus* WT group, $^{\#\#}p<0.01$ *versus* Tg group, and $^{\$\$}p<0.01$ *versus* WT + Hypo group by two-way ANOVA, $n=8$–10 in each group. Values represent the mean ± SEM.

B). However, HO-1, NQO1, γGCL-C, and γGCL-M levels were reduced in the Tg group in the 8- and 14-month-old mice brain compared with the WT group ($p<0.01$; Fig. 8A–E). Importantly, by 8 and 14 months of age, the expression of HO-1, NQO1, γGCL-C, and γGCL-M in the hypoxia-treated WT and Tg mice brain was progressively reduced compared with their control groups without hypoxia treatment ($p<0.01$; Fig. 8A–E). mRNA determination of these NRF2 target genes by RT-PCR confirmed the results (Supplementary Fig. S2).

Intranasal gene delivery of human NRF2 alleviates hypoxia-triggered spatial learning impairment in APP/PS1 mice

To further examine the underlying mechanism of the NRF2-ARE interaction in hypoxia-induced AD-like pathogenesis and investigate the efficacy of NRF2-ARE therapy, we delivered NRF2 intranasally to the AD mouse with a lentiviral vector encoding human NRF2 (LV-NRF2). Lentivirus vectors encoding GFP (LV-GFP) or LV-NRF2 were intranasally administered at weeks 0 and 4 in 2-month-old male APP/PS1 and age-matched WT mice. Six months later, the mice were treated with chronic hypoxia for 2 months. After behavioral tests, the mice were sacrificed, and brains were removed for morphological and biochemical analysis.

First, we evaluated GFP fluorescence localization. As shown in Figure 9A, the viral vector primarily targeted the cell bodies of neurons. Compared with untreated control animals, no obvious histological evidence of side effects or toxicity related to lentiviral transduction was observed (data not shown). Western blot analysis with anti-NRF2 antibody (1: 1000; Abcam, Cambridge, United Kingdom) (Fig. 9B) and ELISA analysis (Fig. 9C) of NRF2 DNA-binding activity

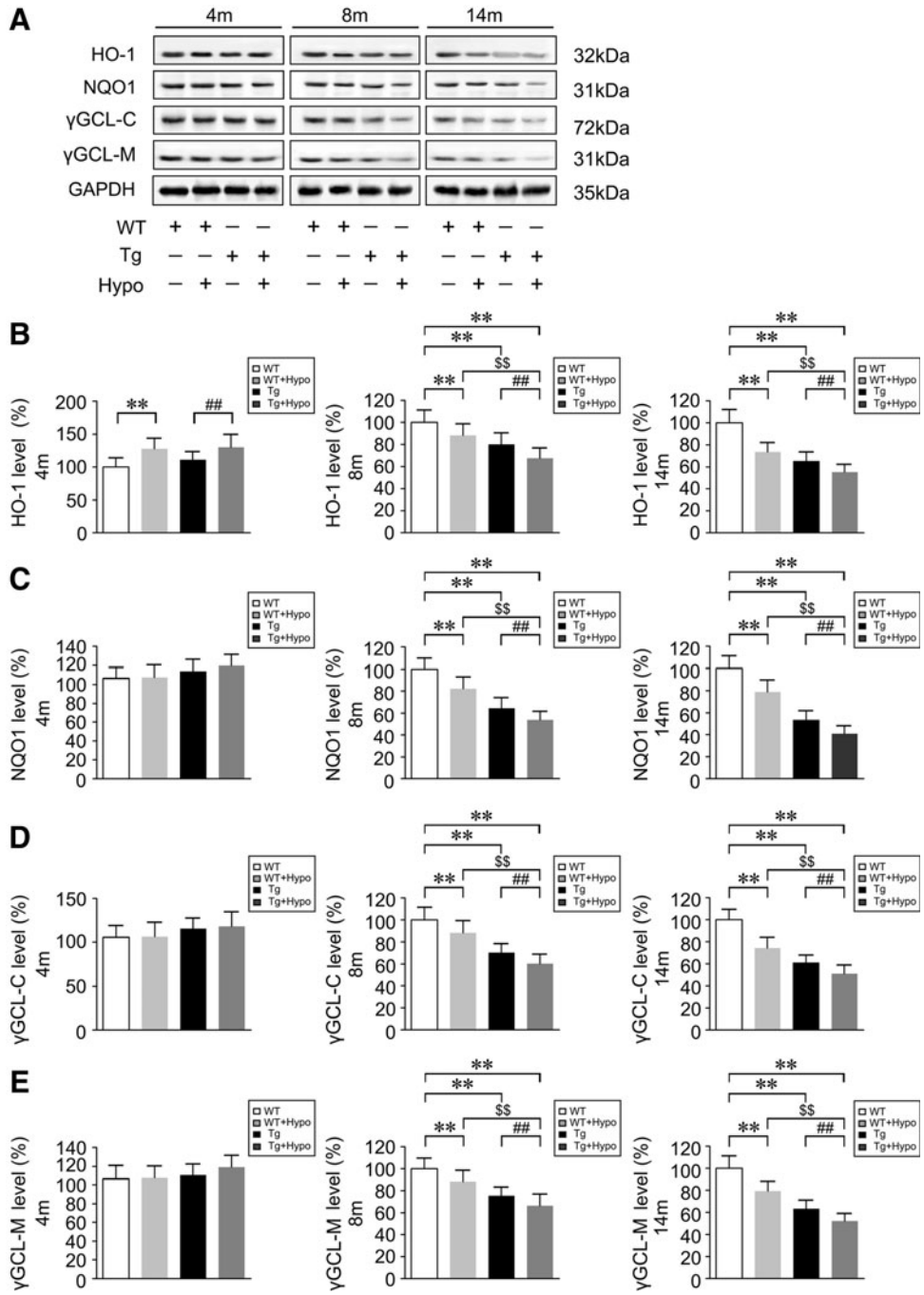

FIG. 8. Chronic hypoxia treatment attenuates NRF2-ARE signals in the aging mouse brain. (A) Representative Western blot images of the NRF2-ARE-driven antioxidants protein, heme oxygenase-1 (HO-1), nicotinamide adenine dinucleotide phosphate quinone oxidoreductase-1 (NQO1), catalytic subunits of γ-glutamyl cysteine ligase (γGCL-C) and modulatory subunits of γ-glutamyl cysteine ligase (γGCL-M) compared with GAPDH in the brains of APP/PS1 transgenic (Tg) and age-matched WT C57BL/6 mice. **(B–E)** Quantification shows the levels of HO-1, NQO1, γGCL-C, and γGCL-M in the mice brain. $^{**}p<0.01$ *versus* WT group, $^{\#\#}p<0.01$ *versus* Tg group, and $^{\$\$}p<0.01$ *versus* WT + Hypo group by two-way ANOVA, $n=8$–10 in each group. Values represent the mean ± SEM.

demonstrated that the levels of cytosolic and nuclear NRF2 levels were increased with LV-NRF2 treatment in WT and Tg groups relative to LV-GFP-treated WT and Tg controls, respectively ($p<0.01$). LV-NRF2 pretreatment diminished hypoxia-triggered down-regulation of NRF2 signaling in the Tg mice brain ($p<0.01$, Fig. 9B, C).

We then examined the protein expression of synaptic markers. As shown in Figure 9D, the levels of SYN, synapsin I, and SNAP-25 were higher in the LV-NRF2 treated group compared with the LV-GFP group in the WT and Tg mice brain ($p<0.01$). Furthermore, under LV-NRF2 intranasal pretreatment, SYN, synapsin I, and SNAP-25 protein expression were higher in hypoxia-treated Tg group (NRF2 + Hypo) relative to Tg mice with GFP + Hypo treatment ($p<0.01$, Fig. 9D). NRF2 gene delivery attenuated the decrease in hypoxia-induced synaptic marker protein expression in the Tg mice brain, suggesting that expression of NRF2 can rescue the hypoxic phenotype associated with AD progression.

The results of the learning and memory assays by MWM and Y-maze tests were consistent with the changes in synaptic marker protein expression. In MWM testing, the escape latency in the 2 days of visible platform trials did not differ among groups, and the third day and fourth day hidden platform tests did not differ as well (data not shown). During the subsequent hidden platform testing, WT mice exhibited

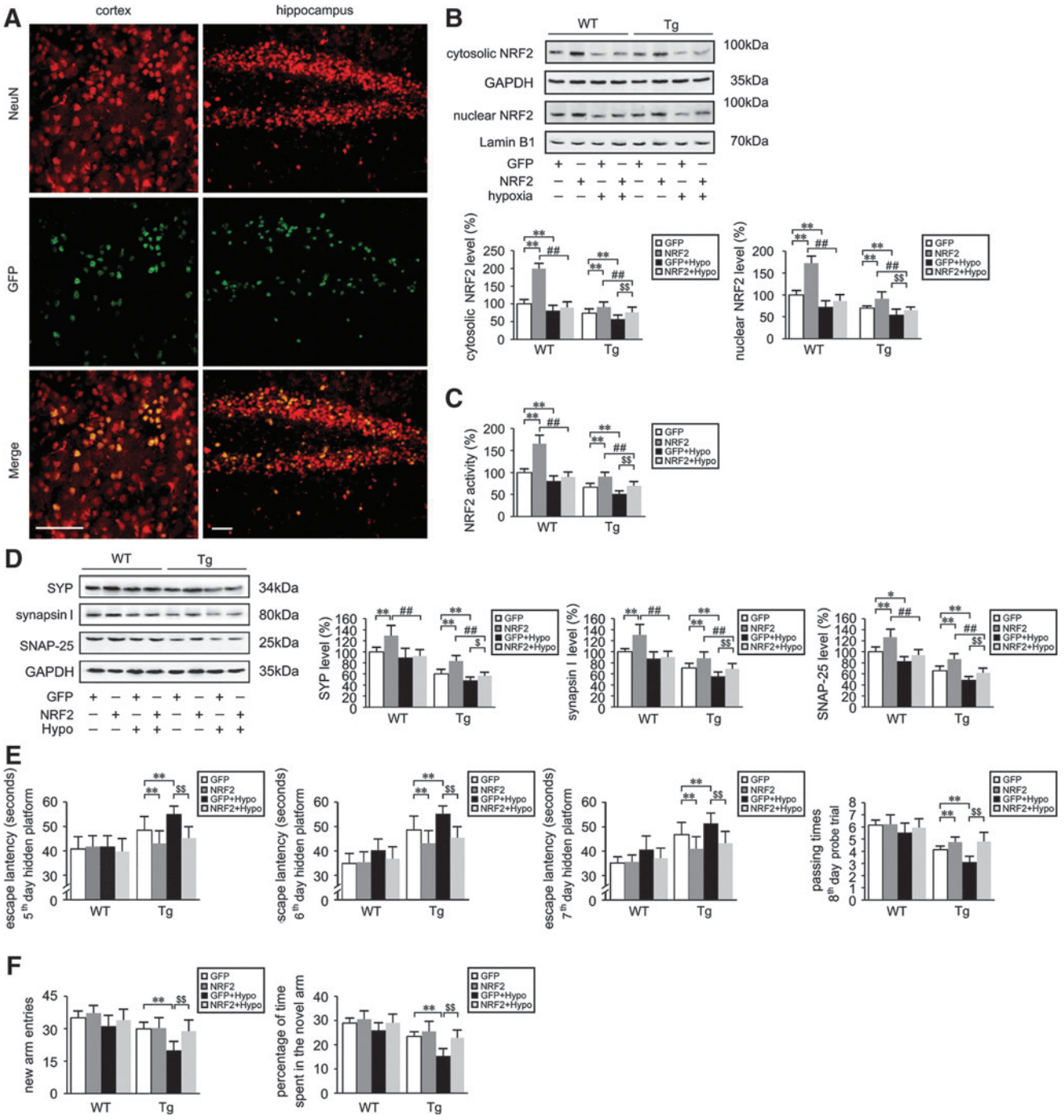

FIG. 9. NRF2 gene transfer lessens spatial learning and memory defects induced by hypoxia treatment in the APP/PS1 mouse. Lentiviral vectors (LV) encoding GFP or human NRF2 were intranasally administered to 2-month-old APP/PS1 transgenic (Tg) and age-matched WT C57BL/6 mice at 0 and 4 weeks. Intranasal treatment with lentivirus vector encoding GFP was used as the control. After 6 months, the mice were treated with hypoxic conditions (Hypo) for 2 months. **(A)** Representative images from brain sections of mice that received intranasal treatment with lentiviral vector encoding GFP. Anti-Neuron-specific nuclear protein (NeuN) antibody was used to identify neurons. GFP fluorescence is colocalized with NeuN. Scale Bar = 50 μm. **(B)** Representative Western blot images of NRF2 in the cytosolic and nuclear fractions in the brains of Tg and WT mice, and compared with GAPDH and Lamin B1, respectively. **(C)** Levels of nuclear NRF2 measured by ELISA. **(D)** Western blots were performed to measure the protein expression of synaptophysin (SYP), synapsin I, and synaptosomal-associated protein 25-kDa (SNAP-25). $^{**}p < 0.01$ *versus* LV-GFP group, $^{\#\#}p < 0.01$ *versus* LV-NRF2 group, and $^{\$\$}p < 0.01$ *versus* GFP + Hypo group by repeated-measures ANOVA, $n = 8$–10 in each group. Values represent the mean ± SEM. **(E)** Spatial learning and memory performance of mice in the MWM test. **(F)** Cognitive behavior of mice subjected to the Y-maze testing. $^{**}p < 0.01$, $^{\$\$}p < 0.01$ by repeated measures ANOVA, $n = 8$–10 in each group. Data are represented as mean ± SEM.

comparable performance ($p > 0.05$, Fig. 9E). However, the mice of the Tg + GFP + Hypo group showed an increase in escape latency compared with the Tg + GFP group from the fifth day to seventh day testing ($p < 0.01$; Fig. 9E). In the Tg mice, NRF2 intranasal pretreatment (Tg + NRF2 + Hypo) alleviated hypoxia-induced increase of escape latency relative to the Tg + GFP + Hypo group ($p < 0.01$; Fig. 9E). In the probe trial on the eighth day, no significant differences were found among the WT groups, whereas NRF2 lentiviral gene transfer significantly lessened the hypoxia-induced poor performance in Tg mice ($p < 0.01$; Fig. 9E). The passing times of mice in the Tg + NRF2 + Hypo treatment group were significantly increased compared with the mice in the Tg + GFP + Hypo group ($p < 0.01$; Fig. 9E). In the Y-maze trial, the new arm entries and percentage of time spent in the novel arm in Tg + NRF2 + Hypo mice were increased compared with Tg + GFP + Hypo mice ($p < 0.01$; Fig. 9F). Taken together, these results indicate that exogenous delivery of NRF2 was able to improve spatial learning in an AD model, and alleviated hypoxia-triggered spatial learning impairment.

Activation of NRF2-ARE upregulates CD36 and lessens hypoxia-induced Aβ clearance and phagocytosis deficiency in the APP/PS1 mouse brain

We first examined the expression levels of the NRF2 targets HO-1, NQO1, γGCL-C, and γGCL-M by Western blot. As shown in Figure 10, after lentivirus-mediated gene delivery of NRF2, the expression of these four potentially protective enzymes was upregulated in both WT and Tg mouse brain tissues ($p < 0.01$; Fig. 10A). Interestingly, in the WT mice, the HO-1, NQO1, and γGCL-C levels of the NRF2 + Hypo group were higher compared with the GFP + Hypo group ($p < 0.01$, Fig. 10A). Most importantly, intranasal treatment with LV-NRF2 lessened the hypoxia-induced

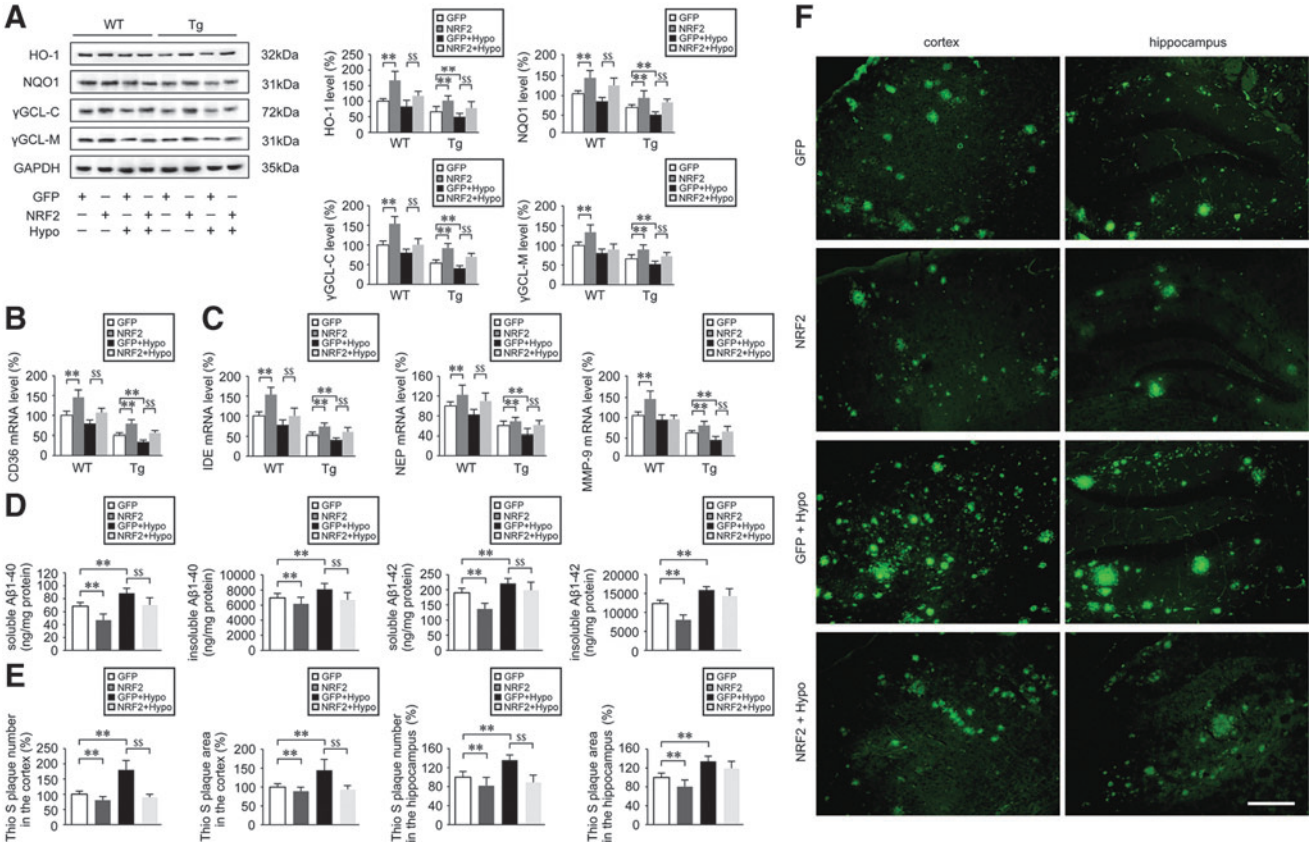

FIG. 10. NRF2-ARE-mediated increase in CD36 alleviates the hypoxia-exacerbated decrease of Aβ clearance and phagocytosis in the brain of APP/PS1 mice. (A) Representative Western blot images of heme oxygenase-1 (HO-1), nicotinamide adenine dinucleotide phosphate quinone oxidoreductase-1 (NQO1), catalytic subunits of γ-glutamyl cysteine ligase (γGCL-C), and modulatory subunits of γ-glutamyl cysteine ligase (γGCL-M) compared with GAPDH in the APP/PS1 transgenic (Tg) and age-matched WT C57BL/6 mouse brain after intranasal treatment using a lentiviral vector (LV) encoding human NRF2 or GFP, and then under control or hypoxic conditions. **(B)** Real-time PCR assays show the relative mRNA expression of CD36 normalized to the level of β-actin in $CD11b^+$ cells of the mouse brain. **(C)** mRNA expression levels of insulin degradation enzyme (IDE), neprilysin (NEP), and matrix metalloproteinase-9 (MMP-9). **(D)** ELISA analyses showing the human Aβ1-40 and Aβ1-42 levels in the mice brain. **(E)** Representative images of Aβ-containing neuritic plaque with Thioflavin S (Thio S) staining in the cerebral cortex and hippocampus. Scale Bar = 50 μm. **(F)** Percentage of Thio S positive staining in the Tg mice brain. $^{**}p < 0.01$ *versus* LV-GFP group, $^{\#\#}p < 0.01$ *versus* LV-NRF2 group, and $^{\$\$}p < 0.01$ *versus* GFP + Hypo group by repeated-measures ANOVA, $n = 8$–10 in each group. Results are expressed as mean ± SEM.

protein reduction of HO-1, NQO1, γGCL-C, and γGCL-M in the Tg mice (Tg + NRF2 + Hypo) compared with the hypoxia-treated Tg mice without NRF2 transduction (Tg + GFP + Hypo; $p < 0.01$, Fig. 10A).

To investigate whether increased NRF2 affected the expression of the Aβ-binding receptor, CD36, we examined CD36 levels in $CD11b^+$ cells isolated from mouse brain tissues by real-time PCR. As illustrated in Figure 10B, NRF2 gene delivery resulted in a significant increase in CD36 mRNA levels in $CD11b^+$ cells isolated from LV-NRF2-treated WT and Tg mouse brain. Gene delivery of NRF2 (Tg + NRF2 + Hypo) alleviated the hypoxia-induced decrease in CD36 expression observed in the WT and Tg mouse brain (Tg + GFP + Hypo; $p < 0.01$, Fig. 10B). Interestingly, CD36 mRNA expression was also increased in the WT + NRF2 mouse brain ($p < 0.01$; Fig. 10B).

To assess the capacity of $CD11b^+$ cells to degrade Aβ after intranasal treatment with NRF2, the expression of three major Aβ-degrading enzymes, IDE, NEP, and MMP-9, was analyzed by real-time PCR. As illustrated in Figure 10C, LV-NRF2 administration increased the mRNA levels of IDE and NEP in WT (WT + NRF2) and Tg mice (Tg + NRF2) compared with WT + GFP and Tg + GFP mice, respectively ($p < 0.01$, Fig. 10C). MMP-9 expression was also significantly increased with NRF2 transduction in WT and Tg mice compared with the control mice (LV-GFP, $p < 0.01$; Fig. 10C). Importantly, NRF2 gene delivery reversed the hypoxia-induced decrease of IDE and NEP mRNA expression and enhanced the expression of these Aβ-degrading enzymes in the WT (Tg + NRF2 + Hypo) and Tg (Tg + NRF2 + Hypo) mice compared with the hypoxia-treated WT (WT + GFP + Hypo) and Tg group (Tg + GFP + Hypo) without NRF2 administration ($p < 0.01$; Fig. 10C). There was no significant difference in the MMP-9 level between WT + NRF2 + Hypo and WT + GFP + Hypo group ($p > 0.05$, Fig. 10C).

We then explored whether NRF2 transduction could alter Aβ burden and affect hypoxia-induced Aβ deposition in the APP/PS1 mouse brain. ELISA showed that LV-NRF2 treatment reduced human soluble and insoluble Aβ1-40 levels ($p < 0.01$), and human soluble Aβ1-42 levels ($p < 0.01$) in the Tg mouse brain (Fig. 10D). The increase in soluble Aβ1-40 and Aβ1-42 triggered by hypoxia was diminished with NRF2 gene delivery ($p < 0.01$, Fig. 10D), and insoluble Aβ1-40 contents were as well. However, there were no statistical differences in the levels of insoluble Aβ1-42 between the Tg + NRF2 + Hypo and Tg + GFP + Hypo group ($p > 0.05$; Fig. 10D). Thioflavin S (Thio S) staining indicated that intranasal administration of LV-NRF2 reduced the Aβ-containing neuritic plaque number and area in the Tg mouse brain ($p < 0.01$; Fig. 10E, F). LV-NRF2 pretreatment reduced the upregulation of neuritic plaque number and area triggered by hypoxia in the cortex (Tg + NRF2 + Hypo) compared with the Tg + GFP + Hypo group ($p < 0.01$; Fig. 10E, F). The number and area of Thio S neuritic plaque in the hippocampus were less in the Tg + NRF2 group relative to Tg + GFP mice ($p < 0.01$, Fig. 10E, F). There was no statistical difference in the plaque area of hippocampus between Tg + NRF2 + Hypo and Tg + GFP + Hypo mice, although the plaque number in Tg + NRF2 + Hypo was less than Tg + GFP + Hypo group. Individual plaques in Tg + GFP + Hypo mouse brains appeared to exhibit a ''dense core'' surrounded by a halo of diffuse amyloid, while the plaques in Tg + NRF2 + Hypo mouse brains had an overall diffuse appearance (Fig. 10F).

Intranasal treatment with NRF2 diminishes ROS and neuroinflammation, and attenuates hypoxia-induced oxidative stress of APP/PS1 mouse brain

To determine the effects of LV-NRF2 administration on hypoxia-induced oxidative stress in the Tg mouse brain, ROS levels were assayed using the CM-H_2DCFDA assay. As illustrated in Figure 11A, ROS levels triggered by hypoxia in the NRF2 pretreated group (Tg + NRF2 + Hypo) were significantly reduced compared with hypoxia-treated Tg mice without NRF2 transduction (Tg + GFP + Hypo; $p < 0.01$, Fig. 11A). LV-NRF2 pretreated WT mice (WT + NRF2 + Hypo) exhibited a resistance to the hypoxia-induced increase in ROS levels compared with WT + GFP + Hypo mice ($p < 0.01$; Fig. 11A).

We then assessed alterations of carbonylated protein and MDA contents in the mouse brain. LV-NRF2 treatment significantly reduced carbonylated protein ($p < 0.01$; Fig. 11B) and MDA generation ($p < 0.01$; Fig. 11C) in the Tg mouse brain. Interestingly, the carbonylated protein and MDA contents from Tg + NRF2 + Hypo mice were markedly reduced compared with the levels from Tg + GFP + Hypo mice brain ($p < 0.01$; Fig. 11B, C). Accordingly, the antioxidant enzyme activities of GSH-PX (Fig. 11D) and CAT (Fig. 11E) were increased with LV-NRF2 intranasal treatment in WT and Tg mice compared with their LV-GFP groups, respectively ($p < 0.01$). In addition, NRF2 gene delivery alleviated hypoxia-induced decrease of GSH-PX activity in Tg + NRF2 + Hypo mice brain compared with Tg + GFP + Hypo group ($p < 0.01$; Fig. 11D), as were the effects on the CAT activity ($p < 0.01$; Fig. 11E).

Inflammation was assessed by analyzing the pro-inflammatory cytokines, IL-1β and TNFα. Real-time PCR assays showed that with NRF2 gene delivery, $CD11b^+$ cells isolated from Tg mouse brain tissues expressed less IL-1β ($p < 0.01$; Fig. 11F) and TNFα mRNA level ($p < 0.01$; Fig. 11H) than the Tg group with LV-GFP treatment. The increase of hypoxia-induced IL-1β levels in Tg + GFP + Hypo mice was diminished with intranasal LV-NRF2 pretreatment (Tg + NRF2 + Hypo) ($p < 0.01$; Fig. 11F), as were the regulations to TNFα levels ($p < 0.01$; Fig. 11H). Effects of NRF2 gene delivery on the resistance to hypoxia-induced IL-1β and TNFα increases were as well in WT mice ($p < 0.01$; Fig. 11F, H). Detection of IL-1β and TNFα levels using ELISA analyses confirmed these results ($p < 0.01$; Fig. 11G, I). We then visualized the distribution of microglia and astrocytes by immunostaining to evaluate the inflammatory response in the WT and Tg mouse brain. As shown in Figure 11J, microglia and astrocytes, detected by anti-CD11b and anti-glial fibrillary acidic protein (GFAP), respectively, formed inflammatory foci and appeared as clusters around florid plaques in the brain of Tg + GFP + Hypo mice. Conversely, microglia and astrocytes expressed less GFAP and CD11b in the brains of Tg + NRF2 + Hypo mice compared with Tg + GFP + Hypo mice.

Discussion

Hypoxia is a crucial risk factor to the onset and progression of AD (8). Chronic hypoxia is always accompanied by robust

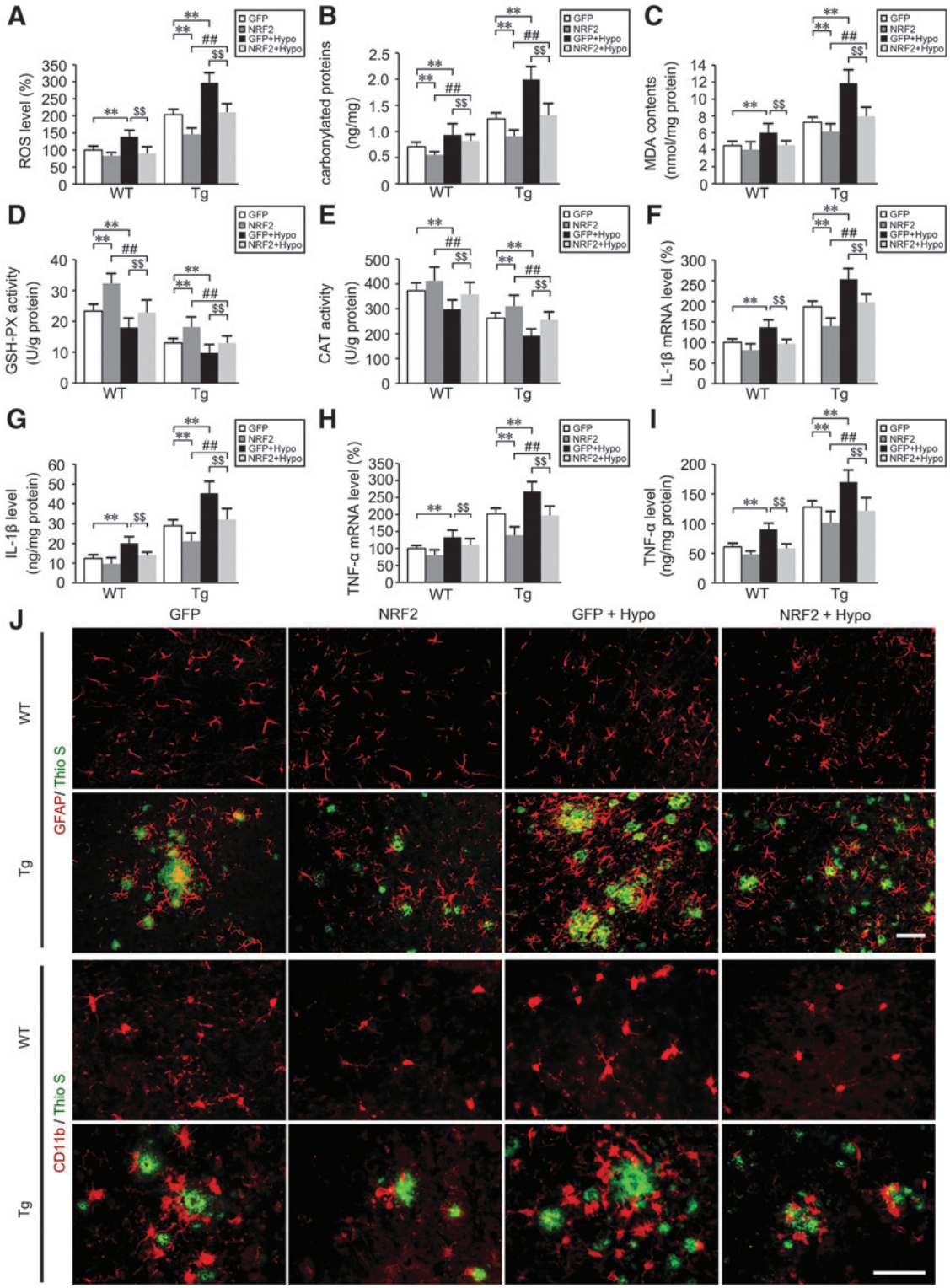

FIG. 11. NRF2 transduction reduces oxidative stress and neuroinflammatory pathological markers in the hypoxia-treated APP/PS1 mouse brain. **(A)** The effects of lentiviral vector (LV) encoding human NRF2 intranasal administration on the reactive oxygen species (ROS) production triggered by hypoxia in the APP/PS1 transgenic (Tg) and age-matched WT C57BL/6 mice brain. **(B)** Alterations in carbonylated proteins in the mice brain. **(C)** Levels of the lipid peroxidation product, malondialdehyde (MDA) in the mice brain. **(D, E)** Activities of antioxidant enzymes, glutathione peroxidase (GSH-PX), and catalase (CAT) were assayed by colorimetry. mRNA and protein expression levels of interleukin-1β (IL-1β) in CD11b^{+} cells from Tg and age-matched WT mice brain were determined by real-time PCR **(F)** and ELISA **(G)**, respectively. **(H)** Relative mRNA expression levels of TNFα were normalized to the levels of β-actin. **(I)** TNFα protein levels were measured by ELISA. **(J)** Frozen sections were stained with anti-CD11b or anti-glial fibrillary acidic protein (GFAP) and Thioflavin-S (Thio S). Scale Bar = 50 μm. $^{**}p < 0.01$ *versus* LV-GFP group, $^{\#\#}p < 0.01$ *versus* LV-NRF2 group, $^{\$\$}p < 0.01$ *versus* GFP + Hypo group, by repeated-measures ANOVA, $n = 8$–10 in each group. Data are represented as mean ± SEM.

synthesis of cytokines, production of related lipids, an increase of ROS, and induction of inflammatory genes (7). These molecular changes may initiate and accelerate AD neural cell degeneration, resulting in a vicious feedback cycle.

Exposure to chronic hypoxia increases oxidative stress and inflammatory events in the aged APP/PS1 mouse brain, worsening the learning and memory deficit

Oxidative stress increases with age through ROS alterations (5). It has been proposed that intracellular ROS is increased under hypoxia, although the directions in which the changes occur are still debated. ROS increases induced by hypoxia are *via* the electron transfer from ubisemiquinone to molecular oxygen (9). ROS excessive accumulation contributes to the expansion of cellular inflammatory responses. Hypoxia-modulated, pathologic gene induction is significantly affected by ROS feedback (8, 77). Meanwhile, free radicals are generated early in the Aβ aggregation stages (70). Conversely, ROS accumulations are sufficient to trigger increasing Aβ production, thereby initiating a vicious cycle (40). It has been shown that hypoxia results in increases of APP levels; the substrate for Aβ and Aβ levels increases *in vivo* (65). Therefore, the Aβ deposition and ROS accumulation under hypoxia conditions might play a key role in the cellular dysfunction. In the present study, the effects of hypoxia on varying ages APP/PS1 and age-matched C57BL/6 mouse brains were examined. Hypoxia induced increasing ROS production and facilitated oxidative stress-induced injury, which were significantly prominent in 8- and 14-month-old APP/PS1 and the 14-month-old WT mice brain. The mRNA levels of IL-1β and TNFα in CD11b$^+$ cells from APP/PS1 mouse brains were markedly increased in hypoxia-treated mice compared with control WT or Tg mice. These pathological injuries were consistent with the deterioration of learning and memory capacity. Using MWM testing, there was no significant difference during the initial 2 days of the learning phase between WT and Tg mice with or without hypoxia treatment, indicating that hypoxia did not alter motivational or motor abilities. Conversely, hypoxia-treated, aging APP/PS1 mice exhibited a significantly slower phase in the later escape latency and probe trials. Aging APP/PS1 mice showed poor cognitive performance in the Y-maze test, especially with hypoxia treatment. The results were consistent with other studies that have been previously reported (72, 78). Further, the hypoxia-induced decrease in the expression of the synaptic markers, SYP, synapsin I, and SNAP-25, confirmed the cognitive deterioration in mice. These data suggest a relationship between the decreased synaptic protein induced by hypoxia treatment and the oxidative stress and inflammatory events. The increase of Aβ levels in the APP/PS1 mouse brain with age might provide the resources for the cellular or molecular changes in the specific neurotransmitter systems.

Progressive down-regulation of CD36 induced by hypoxia is involved in the defective phagocytosis and degradation of microglia to Aβ in the APP/PS1 mouse brain

One of the key roles of microglia in the brain is to serve as specialized sensors for brain pathological alterations. Microglia becomes activated, migrates to and surrounds damaged or dead cells, and then clears cellular debris under pathological stimulation. However, as AD progresses, microglia displays a compromised clearance function (27, 28). It has been proposed that impaired cerebral Aβ clearance is the leading cause of AD (46). CD36, a receptor of microglial expression, appears to be involved in AD pathogenesis (13). Paradoxically, microglia and macrophages isolated from CD36 null mice had a significant reduction of Aβ fibrillar-induced secretion of cytokines and ROS (22). The receptor complex composed of CD36, Aβ, and Toll-like receptors is necessary for the microglia activation to produce ROS and neurotoxicity. The activation requires all three members to be present (66). On the other hand, CD36-deficient macrophages exhibited a significant phagocytic defect (51). Coraci *et al.* observed that CD36 levels were reduced in the microglia of patients with AD, multiple sclerosis, and Parkinson's disease (13). The level of CD36 mRNA in CD11b$^+$ cells from aging AD mice was much less than in age-matched WT littermates (28). In addition, upregulation of CD36 increases Aβ phagocytosis and results in cognitive improvement in the AD mouse model (76). It has been reported that microglia shows age-associated decreases in the CD36 expression, and impairment in Aβ phagocytosis ability is observed at an according age *in vitro* (24). In the present study, microglial cells were isolated with cell markers for microglia, mouse anti-CD11b-coated microbeads. CD36 mRNA levels in CD11b$^+$ cells from APP/PS1 mouse brains were markedly altered. At 4 months of age, CD36 mRNA levels were slightly increased in Tg mice compared with age-matched WT mice, and hypoxia enhanced the increase in the Tg group. It is possible that CD36 activation in the microglia of mouse brain tissues during early AD progression is an attempt to perform Aβ clearance and phagocytosis. However, the levels of CD36 expression were significantly reduced in aging APP/PS1 mouse brain tissues during the time of Aβ generation and deposition. Our results are similar to the work from another group that utilized various age of AD mice and their WT littermates for analyzing microglia function and their expressing receptor (28). Soluble and insoluble Aβ levels were significantly increased in the Tg group compared with the WT group, and hypoxia treatment enhanced CD36 down-regulation in the aging Tg mouse brain. Hypoxia treatment triggered significant reduction of the Aβ-degrading enzymes, NEP, IDE, and MMP-9, and the increases of IL-1β and TNFα levels. Given that microglia exhibited these dysfunctional characteristics, namely the marked reduction in CD36 and Aβ-degrading enzymes and the increase in inflammatory cytokines, it is possible to speculate that hypoxia might contribute to the additional increase of Aβ deposition and oxidative stress, resulting in further AD progression. Our results suggested that the decrease of CD36 expression on microglia with age, especially under hypoxic stimulation, contributed to the loss of their Aβ phagocytosis and clearing capabilities; while microglia continued to produce pro-inflammatory cytokines, resulting in Aβ increasing accumulation. The generation and accumulation of Aβ, in turn, further exaggerate the hypoxia-induced disorders. The defects of the microglia to fulfil the Aβ-clearing functions might be a result of the Aβ-triggered inflammatory response. Thus, targeting the impaired Aβ clearance function of microglia such as upregulating CD36, reducing ROS excessive

production induced by Aβ accumulation and subsequently the decrease of pro-inflammatory cytokines might be considered a potential therapeutic strategy for AD.

Increase of CD36 mediated by NRF2-ARE activation with LV-NRF2 intranasal treatment alleviates neurodegeneration in the APP/PS1 mouse brain, and improves learning and memory capacity of the mouse

The NRF2-ARE pathway appears to contribute to cellular defense against oxidative stress. The lack of NRF2 renders cells increasingly susceptible to oxidative stress *in vitro* (37, 38). It has also been proposed that NRF2 plays a protective role in AD. Activation of NRF2 protects neural cells against Aβ-induced neurotoxicity (35), and NRF2 gene delivery to 9-month-old AD mice improves spatial learning (34). Interestingly, a known antioxidant, acetyl-l-carnitine, prevents hypobaric hypoxia-triggered spatial memory impairment *via* NRF2-mediated cellular defense against oxidative stress (4). A recent study has reported that the activation of NRF2 attenuated chronic hypoxia-induced cardiopulmonary alterations in mice (19). Most importantly, NRF2 directly regulates alternative first exons of CD36 *via* regulation at the ARE (44). Treatment with an NRF2 activator significantly upregulates CD36 and promotes the activation of CD36 macrophage gene expression (32, 49).

In the present study, at 4 months of age, nuclear NRF2 levels in the APP/PS1 mouse brain were increased compared with age-matched WT mice, and hypoxia treatment cause a slight increase compared with controls. Accordingly, expression of the NRF2 target gene, HO-1, was increased in Tg animals relative to WT animals, especially with hypoxia treatment. Low levels of ROS induce the expression of antioxidant defense genes (18). The activation of the NRF2-ARE is likely due to an increase in the antioxidant response. However, the NRF2-ARE pathway was significantly attenuated in aging Tg and age-matched WT mouse brains. Our findings are in agreement with a previous study (35). Furthermore, hypoxia treatment exacerbated the decrease in protein expression of HO-1, NQO1, γGCL-C, and γGCL-M in the aging mouse brain, suggesting an increasing loss of free radical scavenging ability in the aging mouse brain under hypoxic conditions. The high energy demand in the brain is generally accepted. Hypoxia-induced drop in tissue oxygen levels to the point where oxygen demand exceeds supply results in metabolic crisis. The crisis results in tricarboxylic acid cycle inhibition and puts the ongoing physiological functions in danger, and subsequently a severe energy drop (11, 71). The metabolic crisis might be involved in the proposed mechanism of hypoxia-triggered reductions of antioxidant response gene expression in our study.

To test whether the decrease of scavenger receptor, CD36, was involved in the increasing attenuation of the NRF2-ARE signal with hypoxia in the aging APP/PS1 mouse brain, we return to the mouse experiment. LV-NRF2 was delivered intranasally to 2-month-old APP/PS1 and age-matched WT mice. After 6 months, the mice were treated with either hypoxia or control oxygen conditions for 2 months. We observed that NRF2 gene delivery upregulated NRF2-ARE-dependent genes encoding antioxidant proteins and increased CD36 mRNA levels in the microglia from Tg and WT mouse brains. Further, exogenous delivery of NRF2 attenuated the soluble and insoluble Aβ levels, ROS production, carbonyl protein accumulation, and MDA production triggered by hypoxia. Most importantly, upregulation of the NRF2-ARE signal ameliorated the learning and memory defect induced by hypoxia in aging APP/PS1 mice. Current data suggest that restoring decreased NRF2 function can activate antioxidant signaling pathways and affect the clearance of misfolded protein aggregates. NRF2-induced CD36 increase enhances microglial phagocytosis. Further efforts should be made to elucidating the maintenance and efficiency of intranasal LV-NRF2 intervention, the ideal time for effective administration, and the safety so that it might lead to the discovery of new agency for the treatment of AD.

In summary, our data indicate that CD36 upregulation mediated by intranasal LV-NRF2 treatment increases Aβ clearance and phagocytosis associated with oxidative stress and Aβ neurotoxicity. Modulating NRF2 levels in the brain ameliorates the weak antioxidant defense triggered by hypoxia in aged APP/PS1 and WT mice. The NRF2-mediated increase of CD36 protects against hypoxia-induced deterioration of microglia in AD-like pathogenesis.

Materials and Methods

Animals

Male APP/PS1 double-transgenic mice expressing a chimeric mouse/human Swedish mutation amyloid precursor protein (Mo/HuAPP695swe) and a mutant human presenilin 1 (PSEN1dE9) directed to CNS neurons, and WT C57BL/6 mice were obtained from the Jackson Laboratory (West Grove, PA). APP/PS1 mouse secrete a human Aβ peptide because of the ''humanized'' Mo/HuAPP695swe. The mutant of human PSEN1dE9 carrying the exon-9-deleted variant is associated with familial AD. Mice were kept in a controlled environment of 22°C–25°C, 40%–60% relative humidity, and a 12-h light/dark cycle with standard diet and distilled water available *ad libitum*. The study was proved by the ethics committee for laboratory animals of the China Medical University.

Exposure to hypoxia

Experiments were conducted in two phases. In Phase I, hypoxia treatment was performed as previously described (42, 63, 72). Briefly, 2-, 6-, and 12-month-old APP/PS1 transgenic (Tg) mice and age-matched WT mice were randomly divided into either hypoxia or control treatment groups. Mice receiving hypoxia treatment were placed into a 125 ml jar containing normal oxygen conditions. The jar was tightly sealed using a rubber plug and once the first gasping breath was observed, the mouse was immediately removed from the jar. In each experiment, the time at which the first gasp was observed for each mouse was regarded as the tolerance limit. Alteration of hypoxia marker triggered by the hypoxic intervention, HIF1α, was tested (Supplementary Fig. S1 and Supplementary Table S1). Exposure to hypoxic conditions was once daily for 2 months. Body weight and general health of the mouse were monitored daily.

Lentivirus creation and administration

In Phase II, NRF2 was delivered intranasally to APP/PS1 mice using a lentiviral vector encoding human NRF2 (LV-

NRF2) to determine the effect of NRF2 against hypoxia. Enhanced GFP- and NRF2-expressing lentiviruses under the control of a human phosphoglycerate kinase promoter were used for lentiviral gene transfer (36, 75). NRF2 was cloned by excising NRF2 from pCI-NRF2 (41, 75) with 5–10 units of NheI (New England Biolabs, Beverly, MA) and SalI (New England Biolabs), and then was half-blunt ligated into the BamHI-SalI site of the LV-GFP vector, displacing the GFP. The lentiviruses were produced and titrated as previously described (31). The lentiviral vector coding for GFP was used as the control. Two-month-old male APP/PS1 mice and age-matched WT mice were divided into four groups: control (LV-GFP), LV-NRF2, LV-GFP + Hypoxia, and LV-NRF2 + Hypoxia. For intranasal administration, mice were lightly anesthetized with pentobarbital sodium (4 μg/kg body weight). After 15 min, virus particles in 10 μl of sterile PBS (pH 7.4) at a titer of 4×10^8 (34) were delivered intranasally into the right nostril of the mice using a micropipettor with a gel-loading tip (Finnpipette) at week 0. Mice were given the same intranasal treatment at the fourth week. After 6 months, APP/PS1 mice and WT mice were exposed to hypoxia as mentioned earlier for 2 months. At 10 months of age, the mice were assessed for behavioral testing and biochemical assays.

Behavioral testing

Twenty-four hours after the last hypoxia treatment, mice were tested using the MWM and Y-maze. The MWM (55) was used to test spatial memory. The apparatus (ZH0065, Zhenghua Bioequipments; Zhejiang, Jiangsu, China) was a circular tank that was equipped with a digital pick-up camera and a computer program to semi-automatically monitor the animal behavior and analyze data. Briefly, mice had 2 days of pretraining to remember the visible platform placed in the center of the northwest quadrant in the tank, after which they underwent a 5-day navigation test to find a hidden platform submerged 1 cm below the water surface. Each mouse was subjected to three trials with a 1 min inter-trial interval per day. The escape latency to the platform and the path length of each trial was recorded. On the eighth day, the platform was removed for the probe trial. The passing times that the mouse crossed the center where the platform was placed previously were recorded.

The Y-Maze Test (14) was used for testing spatial memory and learning. Briefly, three identical arms of the maze (Muromachi Kikai, Tokyo, Japan) were randomly designated as the start arm, novel arm, or other arm. All mice were subjected to two trials separated by a 1-h, inter-trial interval. In the first training trial, the mice were allowed to explore the starting arm and the other arm for 10 min. Then, for the second retention trial, mice were placed back in the maze in the same starting arm and allowed to explore for 5 min with free access to all three arms. The number of entries and percentage of time spent in the novel arm that mice examined were analyzed.

Preparation of brain samples

After behavioral testing, mice were deeply anesthetized with sodium pentobarbital (50 mg/kg, intraperitoneally). Animals were then transcardially perfused with ice-cold 0.9% saline and sacrificed by decapitation. The brains were immediately removed and dissected in half on an ice-cold board. One half was prepared for morphological assessment, and the other half was prepared for biochemical assays.

Isolation of microglia

The isolation of microglia from adult mouse brains was performed as previously described (28). Briefly, mouse brain tissue was placed into Roswell Park Memorial Institute (RPMI) 1640 medium (Gibco, Grand Island, NY) containing 2 m*M* L-glutamine (no phenol red), 2.0 U/ml Dispase (Gibco), and 0.2% Collagenase Type 3 (Worthington Biochemicals, Lakewood, NJ). After mincing with sterile razor blades, tissues were digested for 45 min at 37°C, followed by addition of DNase I, grade II (Roche Applied Science, Indianapolis, IN) at a concentration of 40 U/ml for another 15 min. The digestion was terminated by adding 20-ml Hanks Balanced Salt Solution containing 2 m*M* EDTA and 2% fetal bovine serum. The samples were then sequentially triturated and passed through a filter. The cells were collected and resuspended in RPMI 1640 with L-glutamine. After adding Physiologic Percoll (Sigma-Aldrich, St. Louis, MO), the samples were centrifuged at 850 *g* for 45 min. The cell pellet was resuspended in RPMI and sequentially passed through a 70-μm filter and a 40-μm filter (Fisher Scientific, Waltham, MA). The cells were then incubated with cell markers for microglia, mouse anti-CD11b-coated microbeads (Miltenyi Biotech, Auburn, CA) for 20 min at 12°C. After washing, the bead-cell pellet was resuspended in PBS containing 0.5% BSA, 2 m*M* EDTA and then passed over a magnetic MACS Cell Separation column (Miltenyi Biotec, Bergisch Gladbach, Germany) so that CD11b-positive ($CD11b^+$) cells were separated from CD11b-negative cells. Flow-through was collected, and the column was rinsed with PBS. $CD11b^+$ cells were eluted, and the resulting cells were collected by centrifugation.

Real-time PCR

Total RNA from mouse brain or $CD11b^+$ cells of each sample was extracted using Trizol (Invitrogen, Grand Island, NY) according to the manufacturer's instructions. The integrity of the RNA was analyzed by agarose gel electrophoresis. The yield of total RNA was determined by assessing the absorbance (260 nm: 280 nm ratio). A total of 3 μg RNA was reverse transcribed using the Prime Script RT Reagent Kit (Takara, Otsu, Japan). The reverse-transcription conditions were 37°C for 15 min followed by 85°C for 5 s. For real-time RT-PCR, each specific gene product was amplified with SYBR Green PCR Master mix (Applied Biosystems, Inc. (ABI), Foster City, CA) using an ABI 7300 Sequence Detection System. Each reaction mixture contained 50 ng of cDNA. Cycling conditions included a preincubation of 50°C for 2 min, DNA polymerase activation at 95°C for 5 min, followed by 30 cycles of denaturing at 95°C for 30 s, and annealing and extension at 58°C for 30 s. Each cDNA sample was assayed in triplicate. Primer sequences used for PCR quantification were as follows: NRF2: forward, 5′-TGG ACG GGA CTA TTG AAG GCT G-3′, reverse, 5′-GCC GCC TTT TCA GTA GAT GGA GG-3′; CD36: forward, 5′-TTT CCT CTG ACA TTT GCA GGT CTA-3′; reverse, 5′-AAA GGC ATT GGC TGG AAG AA-3′; IL-1β: forward, 5′-ACC TGT CCT GTG TAA TGA AAG ACG-3′; reverse, 5′-TGG GTA TTG CTT GGG ATC CA-3′; TNFα:

forward, 5′-GCA CAG AAA GCA TGA CCC G-3′; reverse, 5′-GCC CCC CAT CTT TTG GG-3′; IDE: forward, 5′-GAA GAC AAA CGG GAA TAC CGT G-3′; reverse, 5′-CCG CTG AGG ACT TGT CTG TG; NEP: forward, 5′-GCA GCC TCA GCC GAA ACT AC-3′; reverse, 5′-CAC CGT CTC CAT GTT GCA GT-3′; MMP-9: forward, 5′-GCC ATG CAC TGG GCT TAG AT-3′; reverse, 5′-TCT TTA TTC AGA GGG AAG CCC TC-3′; β-actin: forward, 5′-GTA TGA CTC CAC TCA CGG CAA A-3′, reverse, 5′-GGT CTC GCT CCT GGA AGA TG-3′. Primer sequences used for NRF2 target genes and HIF1α determination were displayed in Supplementary Table S1. Expression was calculated using threshold cycle (Ct) values normalized to β-actin, and relative differences between control and treatment groups were expressed as a percentage relative to control.

Measurement of ROS production

Determination of ROS levels in the cortex of the mouse brain was performed as previously described with minor modifications (25). Briefly, cortices of mice brain were homogenized in ice-cold 10 m*M* Tris-HCl buffer (pH 7.4) (1: 10, w/v) containing 100 m*M* sucrose, 10 m*M* EDTA, and then centrifuged at 800 *g* for 5 min. The supernatant was collected and centrifuged at 1000 *g* for 10 min. The cell pellets were suspended in cold PBS and counted using trypan blue. Cells (2×10^6/ml) were incubated in a HEPES-Tris medium (HT) containing 1 μ*M* 5-(and-6)-chloromethyl-2′, 7′-dichlorodihydrofluorescein diacetate ([CM-H_2DCFDA]; Molecular Probes, Invitrogen, Carlsbad, CA), 132 m*M* NaCl, 4.2 m*M* KCl, 1 m*M* $CaCl_2$, 1 m*M* $MgCl_2$, and 10 m*M* HEPES (pH 7.4) for 30 min at 25°C with protection from light. Negative controls were incubated with PBS. After removing the supernatant by centrifugation at 1000 *g* for 10 min, samples were then returned to HT medium at 25°C for 10 min. After lysis with lysis buffer containing 1% Nonidet P-40, 150 m*M* NaCl, and 50 m*M* Tris (pH 8.0), the supernatants were collected by centrifugation at 19,000 *g* for 10 min (4°C). The samples were diluted with a fourfold volume of deionized water and measured with a VersaFluor Fluorometer System (Bio-Rad Laboratories, Hercules, CA) using an excitation filter of 490 nm.

Assays of antioxidant enzyme activity

Mouse brain cortices were weighed, and a ninefold volume of phosphate-buffered saline was added. Samples were then ground gently at 4°C. Total protein levels were measured using a UV 1700 PharmaSpec ultraviolet spectrophotometer (SHIMADZU, Tokyo, Japan). GSH-PX and CAT activity in tissue homogenates was determined by colorimetry using suitable kits (Nanjing Jiancheng Bioengineering Institute, Nanjing, Jiangsu, China). The absorbance was recorded at 412 and 240 nm for GSH-PX and CAT, respectively.

Measurement of protein carbonyl groups and lipid peroxidation products

Carbonyl proteins were analyzed as previously described 29. Briefly, protein samples were incubated with an equal volume of 0.1% 2, 4-dinitrophenylhydrazine in 2 *M* HCl for 1 h at room temperature. Then, 20% trichloroacetic acid (TCA) was added to precipitate proteins. After extraction with ethanol/ethyl acetate (1:1) thrice, the precipitate was placed in the lysates containing 8 *M* guanidine hydrochloride, 13 m*M* EDTA, and 133 m*M* Tris (pH 7.4). The absorbance was read at 365 nm. Data were expressed as the quantity of carbonyl protein formed (nmol) per mg of total protein.

The quantity of lipid peroxidation product, MDA, was determined using the MDA Detection Kit (Nanjing Jiancheng Bioengineering Institute, Nanjing, Jiangsu, China). Precipitation of MDA with thiobarbituric acid produces a red product with a maximum absorption peak at 532 nm.

Western blot

Mouse brain tissues were homogenized, lysed in RIPA buffer (150 m*M* NaCl, 1% Nonidet P-40, 0.5% deoxycholic acid, 0.1% SDS, and 50 m*M* Tris, pH 8.0) containing a protease inhibitor cocktail (Sigma-Aldrich), and centrifuged at 15,000 *g* for 30 min at 4°C. The resulting supernatants were collected. Total protein concentrations were determined using the UV 1700 PharmaSpec ultraviolet spectrophotometer. A total of 30 μg of protein was then separated by 10% SDS polyacrylamide gels. The separated proteins were transferred to PVDF membranes (Millipore, Billerica, MA). After blocking in 5% nonfat milk in Tris-buffered saline (TBS) containing 0.05% Tween-20 for 1 h, transferred PVDF membranes were incubated with primary antibodies at 4°C overnight as follows: mouse anti-HIF1α (1: 800; Abcam), rabbit anti-synapsin I (1: 1000; Millipore), rabbit anti-synaptophysin (SYP; 1: 2000; Abcam), rabbit anti-synaptosomal-associated protein 25-kDa (SNAP-25; 1: 1000; Abcam), rabbit anti-NRF2 (1: 1000; Abcam), goat anti-HO-1 (1: 1000; Santa Cruz Biotechnology, Santa Cruz, CA), goat anti-NQO1 (1: 1000; Santa Cruz Biotechnology), rabbit-anti-γGCL-M (1: 800; Santa Cruz Biotechnology), rabbit-anti-γGCL-C (1: 500; Santa Cruz Biotechnology), mouse anti-GAPDH (1:10,000; Kangchen Biotech, Shanghai, China), and rabbit anti-lamin B1 antibody (1: 1000; Abcam). Immunoblots were washed and incubated with the appropriate species-specific horseradish peroxidase-conjugated secondary antibody (1: 5000; Santa Cruz Biotechnology) at room temperature for 1 h. The immunological complexes were visualized with enhanced chemiluminescence substrate (ECL, Amersham Biosciences) using the ChemiDoc XRS system and the accompanying Quantity One software (Bio-Rad Laboratories). Signal intensities data were quantified using Image-pro Plus 6.0 analysis software. Data are expressed as the relative differences between samples after normalization to GAPDH expression.

Immunostaining

Frozen sections (6 μm) of the mouse brain were treated with 5% bovine serum albumin for 1 h, and then incubated with either rabbit anti-glial fibrillary acidic protein (GFAP, 1: 100; Santa Cruz Biotechnology) or mouse anti-CD11b (1: 100; Serotec, Kidlington, Oxford, United Kimgdom) overnight at 4°C. After washes, sections were incubated with Alexa Fluor 568-cojugated secondary antibody (1: 100; Invitrogen) at room temperature for 2 h. After rinsing, sections were treated with fresh, 1% filtered, aqueous Thioflavin-S (Sigma-Aldrich) for 5 min. The slides were then mounted, cover-slipped, and examined with a confocal laser scanning microscope (Model SP2; Leica, Wetzlar, Germany). Images

were analyzed using Nikon EclipseNet and Image J software (National Institutes of Health, Bethesda, MD). For Aβ immunostaining, brain sections were incubated with mouse anti-Aβ antibody (1: 500; Sigma-Aldrich) and then with biotinylated IgG (1: 200) for 1 h, followed by incubation with streptavidin peroxidase for 30 min. After thorough rinses, the sections were treated with 0.025% 3,3-diaminobenzidine plus 0.0033% H_2O_2 in TBS for 5 min. The stained sections were dehydrated, cleared, and mounted with neutral balsam. Sections were examined, and images were obtained with an Olympus microscope (Model DP71).

NRF2 extract preparation

Cytosolic and nuclear extracts of NRF2 were prepared (58) using a nuclear extract kit (Active Motif, Inc., Carlsbad, CA). Briefly, the frontal cortex of mouse brains was homogenized in 1 ml of ice-cold hypotonic buffer A (10 m*M* HEPES [pH 7.9], 10 m*M* KCl, 2 m*M* $MgCl_2$, 1 m*M* dithiothreitol, 0.1 m*M* EDTA, and 0.1 m*M* phenylmethylsulfonyl-fluoride [PMSF]). The samples were centrifuged at 14,000 *g* for 2 min. The supernatant was collected as a cytosolic fraction. The precipitates were washed with Buffer A plus 40 μl of 10% Nonidet (NP-40). Pellets were resuspended in an ice-cold, hypertonic, nuclear extract Buffer B (50 m*M* HEPES (pH 7.9), 50 m*M* KCl, 300 m*M* NaCl, 0.1 m*M* EDTA, 0.5 m*M* Dithiothreitol, 0.1 m*M* PMSF, and 20% glycerol) and centrifuged at 14,000 *g* for 5 min. The supernatant containing nuclear proteins was collected.

Sandwich ELISA

For Aβ detection, ELISA-based assays were performed as previously described 73. Briefly, the cortex of mice brain was homogenized in either ice-cold 20 m*M* Tris pH 8.5 (soluble) or 5 *M* guanidine HCl/50 m*M* Tris-HCl, pH 8.0 (insoluble). The homogenates were diluted with dilution buffer plus protease inhibitor cocktail (Sigma-Aldrich) and thoroughly ground with a hand-held motor. After centrifugation at 15,000 *g* for 30 min at 4°C, the supernatants were collected. Aβ1-40 and Aβ1-42 levels were determined using mouse or human Aβ1-40 ELISA kits (Invitrogen) and Aβ1-42 ELISA kits (Invitrogen), respectively, according to the manufacturer's instructions. The absorbance was recorded at 450 nm using a 96-well plate reader.

NRF2 nuclear proteins isolated from mouse brain tissues were obtained by the method described earlier. NRF2 DNA-binding activity was determined using the TransAM ELISA-kit (Active Motif, Inc.). The absorbance was read at 450 nm. IL-1β and TNFα levels were measured by ELISA using the mouse IL-1β V-PLEX Plus Kit (Meso Scale Discovery, Rockville, MD) and mouse TNFα V-PLEX Plus Kit (Meso Scale Discovery), respectively, according to the manufacturer's instructions. Briefly, mouse brain cortices were homogenized using RIPA buffer containing a protease inhibitor cocktail (Sigma-Aldrich). The supernatants were collected by centrifugation at 15,000 *g* for 30 min at 4°C. The protein concentrations were measured, and 50 μl of each PBS soluble fraction was loaded per well on the plate. The samples were incubated at 22°C with shaking (1000 rpm) for 2 h. Cytokine levels were normalized to total protein content.

Statistical analysis

All values were represented as mean ± standard error of the mean (SEM). Statistical significance between groups was determined by using *t* test or analyses of variance with *post hoc* Fisher's protected least-significant difference. $p < 0.05$ was considered significant.

Acknowledgments

The study was supported by grants from the Natural Science Foundation of China (Nos. 81100808, 81071004, and 81100810), the China Postdoctoral Science Foundation (Nos. 201104615, 2012 M510849, and 2013T60304), and the Specialized Research Fund for the Doctoral Program of Higher Education of China (No. 20112104120010).

Author Disclosure Statement

The authors have no conflicting financial interests.

References

1. Aliev G, Smith MA, Seyidov D, Neal ML, Lamb BT, Nunomura A, Gasimov EK, Vinters HV, Perry G, Lamanna JC, and Friedland RP. The role of oxidative stress in the pathophysiology of cerebrovascular lesions in Alzheimer's disease. *Brain Pathol* 12: 21–35, 2002.
2. Bao Y, Qin L, Kim E, Bhosle S, Guo H, Febbraio M, Haskew-Layton RE, Ratan R, and Cho S. CD36 is involved in astrocyte activation and astroglial scar formation. *J Cereb Blood Flow Metab* 32: 1567–1577, 2012.
3. Bard F, Cannon C, Barbour R, Burke RL, Games D, Grajeda H, Guido T, Hu K, Huang J, Johnson-Wood K, Khan K, Kholodenko D, Lee M, Lieberburg I, Motter R, Nguyen M, Soriano F, Vasquez N, Weiss K, Welch B, Seubert P, Schenk D, and Yednock T. Peripherally administered antibodies against amyloid beta-peptide enter the central nervous system and reduce pathology in a mouse model of Alzheimer disease. *Nat Med* 6: 916–919, 2000.
4. Barhwal K, Hota SK, Jain V, Prasad D, Singh SB, and Ilavazhagan G. Acetyl-l-carnitine (ALCAR) prevents hypobaric hypoxia-induced spatial memory impairment through extracellular related kinase-mediated nuclear factor erythroid 2-related factor 2 phosphorylation. *Neuroscience* 161: 501–514, 2009.
5. Barja G. Free radicals and aging. *Trends Neurosci* 27: 595–600, 2004.
6. Barnwell JW, Asch AS, Nachman RL, Yamaya M, Aikawa M, and Ingravallo P. A human 88-kD membrane glycoprotein (CD36) functions *in vitro* as a receptor for a cytoadherence ligand on Plasmodium falciparum-infected erythrocytes. *J Clin Invest* 84: 765–772, 1989.
7. Bazan NG and Lukiw WJ. Cyclooxygenase-2 and presenilin-1 gene expression induced by interleukin-1beta and amyloid beta 42 peptide is potentiated by hypoxia in primary human neural cells. *J Biol Chem* 277: 30359–30367, 2002.
8. Bazan NG, Palacios-Pelaez R, and Lukiw WJ. Hypoxia signaling to genes: significance in Alzheimer's disease. *Mol Neurobiol* 26: 283–298, 2002.
9. Bell EL, Klimova TA, Eisenbart J, Moraes CT, Murphy MP, Budinger GR, and Chandel NS. The Qo site of the mitochondrial complex III is required for the transduction of hypoxic signaling via reactive oxygen species production. *J Cell Biol* 177: 1029–1036, 2007.
10. Calabrese V, Cornelius C, Dinkova-Kostova AT, Calabrese EJ, and Mattson MP. Cellular stress responses, the hormesis paradigm, and vitagenes: novel targets for therapeutic

intervention in neurodegenerative disorders. *Antioxid Redox Signal* 13: 1763–1811, 2010.
11. Carvalho C, Correia SC, Santos RX, Cardoso S, Moreira PI, Clark TA, Zhu X, Smith MA, and Perry G. Role of mitochondrial-mediated signaling pathways in Alzheimer disease and hypoxia. *J Bioenerg Biomembr* 41: 433–440, 2009.
12. Chang S, Jiang X, Zhao C, Lee C, and Ferriero DM. Exogenous low dose hydrogen peroxide increases hypoxia-inducible factor-1alpha protein expression and induces preconditioning protection against ischemia in primary cortical neurons. *Neurosci Lett* 441: 134–138, 2008.
13. Coraci IS, Husemann J, Berman JW, Hulette C, Dufour JH, Campanella GK, Luster AD, Silverstein SC, and El-Khoury JB. CD36, a class B scavenger receptor, is expressed on microglia in Alzheimer's disease brains and can mediate production of reactive oxygen species in response to beta-amyloid fibrils. *Am J Pathol* 160: 101–112, 2002.
14. Crouch PJ, Hung LW, Adlard PA, Cortes M, Lal V, Filiz G, Perez KA, Nurjono M, Caragounis A, Du T, Laughton K, Volitakis I, Bush AI, Li QX, Masters CL, Cappai R, Cherny RA, Donnelly PS, White AR, and Barnham KJ. Increasing Cu bioavailability inhibits Abeta oligomers and tau phosphorylation. *Proc Natl Acad Sci U S A* 106: 381–386, 2009.
15. D'archivio M, Scazzocchio B, Filesi C, Vari R, Maggiorella T, Sernicola L, Santangelo C, Giovannini C, and Masella R. Oxidised LDL up-regulate CD36 expression by the Nrf2 pathway in 3T3-L1 preadipocytes. *FEBS Lett* 582: 2291–2298, 2008.
16. Desmond DW, Moroney JT, Sano M, and Stern Y. Incidence of dementia after ischemic stroke: results of a longitudinal study. *Stroke* 33: 2254–2260, 2002.
17. Donovan EL, Mccord JM, Reuland DJ, Miller BF, and Hamilton KL. Phytochemical activation of Nrf2 protects human coronary artery endothelial cells against an oxidative challenge. *Oxidative Med Cell Longev* 2012: 132931, 2012.
18. Dröge W. Free radicals in the physiological control of cell function. *Physiol Rev* 82: 47–95, 2002.
19. Eba S, Hoshikawa Y, Moriguchi T, Mitsuishi Y, Satoh H, Ishida K, Watanabe T, Shimizu T, Shimokawa H, Okada Y, Yamamoto M, and Kondo T. The nuclear factor erythroid 2-related factor 2 activator oltipraz attenuates chronic hypoxia-induced cardiopulmonary alterations in mice. *Am J Respir Cell Mol Biol* 49: 324–333, 2013.
20. Eftekharzadeh B, Maghsoudi N, and Khodagholi F. Stabilization of transcription factor Nrf2 by tBHQ prevents oxidative stress-induced amyloid beta formation in NT2N neurons. *Biochimie* 92: 245–253, 2010.
21. El Khoury J, Hickman SE, Thomas CA, Loike JD, and Silverstein SC. Microglia, scavenger receptors, and the pathogenesis of Alzheimer's disease. *Neurobiol Aging* 19: S81–S84, 1998.
22. El Khoury JB, Moore KJ, Means TK, Leung J, Terada K, Toft M, Freeman MW, and Luster AD. CD36 mediates the innate host response to beta-amyloid. *J Exp Med* 197: 1657–1666, 2003.
23. Febbraio M, Hajjar DP, and Silverstein RL. CD36: a class B scavenger receptor involved in angiogenesis, atherosclerosis, inflammation, and lipid metabolism. *J Clin Invest* 108: 785–791, 2001.
24. Floden AM and Combs CK. Microglia demonstrate age-dependent interaction with amyloid-beta fibrils. *J Alzheimer's Dis* 25: 279–293, 2011.
25. Flora SJ, Bhatt K, and Mehta A. Arsenic moiety in gallium arsenide is responsible for neuronal apoptosis and behavioral alterations in rats. *Toxicol Appl Pharmacol* 240: 236–244, 2009.
26. Giordano FJ. Oxygen, oxidative stress, hypoxia, and heart failure. *J Clin Invest* 115: 500–508, 2005.
27. Heneka MT, Nadrigny F, Regen T, Martinez-Hernandez A, Dumitrescu-Ozimek L, Terwel D, Jardanhazi-Kurutz D, Walter J, Kirchhoff F, Hanisch UK, and Kummer MP. Locus ceruleus controls Alzheimer's disease pathology by modulating microglial functions through norepinephrine. *Proc Natl Acad Sci U S A* 107: 6058–6063, 2010.
28. Hickman SE, Allison EK, and El Khoury J. Microglial dysfunction and defective beta-amyloid clearance pathways in aging Alzheimer's disease mice. *J Neurosci* 28: 8354–8360, 2008.
29. Hipkiss AR, Brownson C, and Carrier MJ. Carnosine, the anti-ageing, anti-oxidant dipeptide, may react with protein carbonyl groups. *Mech Ageing Dev* 122: 1431–1445, 2001.
30. Hirano K, Kuwasako T, Nakagawa-Toyama Y, Janabi M, Yamashita S, and Matsuzawa Y. Pathophysiology of human genetic CD36 deficiency. *Trends Cardiovasc Med* 13: 136–141, 2003.
31. Hurttila H, Koponen JK, Kansanen E, Jyrkkänen HK, Kivelä A, Kylätie R, Ylä-Herttuala S, and Levonen AL. Oxidative stress-inducible lentiviral vectors for gene therapy. *Gene Ther* 15: 1271–1279, 2008.
32. Ishii T, Itoh K, Ruiz E, Leake DS, Unoki H, Yamamoto M, and Mann GE. Role of Nrf2 in the regulation of CD36 and stress protein expression in murine macrophages: activation by oxidatively modified LDL and 4-hydroxynonenal. *Circ Res* 94: 609–616, 2004.
33. Itoh K, Chiba T, Takahashi S, Ishii T, Igarashi K, Katoh Y, Oyake T, Hayashi N, Satoh K, Hatayama I, Yamamoto M, and Nabeshima Y. An Nrf2/small Maf heterodimer mediates the induction of phase II detoxifying enzyme genes through antioxidant response elements. *Biochem Biophys Res Commun* 236: 313–322, 1997.
34. Kanninen K, Heikkinen R, Malm T, Rolova T, Kuhmonen S, Leinonen H, Ylä-Herttuala S, Tanila H, Levonen AL, Koistinaho M, and Koistinaho J. Intrahippocampal injection of a lentiviral vector expressing Nrf2 improves spatial learning in a mouse model of Alzheimer's disease. *Proc Natl Acad Sci U S A* 106: 16505–16510, 2009.
35. Kanninen K, Malm TM, Jyrkkänen HK, Goldsteins G, Keksa-Goldsteine V, Tanila H, Yamamoto M, Ylä-Herttuala S, Levonen AL, and Koistinaho J. Nuclear factor erythroid 2-related factor 2 protects against beta amyloid. *Mol Cell Neurosci* 39: 302–313, 2008.
36. Koponen JK, Kekarainen T, E Heinonen S, Laitinen A, Nystedt J, Laine J, and Ylä-Herttuala S. Umbilical cord blood-derived progenitor cells enhance muscle regeneration in mouse hindlimb ischemia model. *Mol Ther* 15: 2172–2177, 2007.
37. Lee JM, Calkins MJ, Chan K, Kan YW, and Johnson JA. Identification of the NF-E2-related factor-2-dependent genes conferring protection against oxidative stress in primary cortical astrocytes using oligonucleotide microarray analysis. *J Biol Chem* 278: 12029–12038, 2003.
38. Lee JM, Shih AY, Murphy TH, and Johnson JA. NF-E2-related factor-2 mediates neuroprotection against mitochondrial complex I inhibitors and increased concentrations of intracellular calcium in primary cortical neurons. *J Biol Chem* 278: 37948–37956, 2003.

39. Leissring MA, Farris W, Chang AY, Walsh DM, Wu X, Sun X, Frosch MP, and Selkoe DJ. Enhanced proteolysis of beta-amyloid in APP transgenic mice prevents plaque formation, secondary pathology, and premature death. *Neuron* 40: 1087–1093, 2003.
40. Leuner K, Schütt T, Kurz C, Eckert SH, Schiller C, Occhipinti A, Mai S, Jendrach M, Eckert GP, Kruse SE, Palmiter RD, Brandt U, Drose S, Wittig I, Willem M, Haass C, Reichert AS, and Müller WE. Mitochondrion-derived reactive oxygen species lead to enhanced amyloid beta formation. *Antioxid Redox Signal* 16: 1421–1433, 2012.
41. Levonen AL, Inkala M, Heikura T, Jauhiainen S, Jyrkkänen HK, Kansanen E, Määttä K, Romppanen E, Turunen P, Rutanen J, and Ylä-Herttuala S. Nrf2 gene transfer induces antioxidant enzymes and suppresses smooth muscle cell growth *in vitro* and reduces oxidative stress in rabbit aorta *in vivo*. *Arterioscler Thromb Vasc Biol* 27: 741–747, 2007.
42. Li L, Zhang X, Yang D, Luo G, Chen S, and Le W. Hypoxia increases Abeta generation by altering beta- and gamma-cleavage of APP. *Neurobiol Aging* 30: 1091–1098, 2009.
43. Liu Y, Liu F, Iqbal K, Grundke-Iqbal I, and Gong CX. Decreased glucose transporters correlate to abnormal hyperphosphorylation of tau in Alzheimer disease. *FEBS Lett* 582: 359–364, 2008.
44. Maruyama A, Tsukamoto S, Nishikawa K, Yoshida A, Harada N, Motojima K, Ishii T, Nakane A, Yamamoto M, and Itoh K. Nrf2 regulates the alternative first exons of CD36 in macrophages through specific antioxidant response elements. *Arch Biochem Biophys* 477: 139–145, 2008.
45. Mattson MP. Cellular actions of beta-amyloid precursor protein and its soluble and fibrillogenic derivatives. *Physiol Rev* 77: 1081–1132, 1997.
46. Mawuenyega KG, Sigurdson W, Ovod V, Munsell L, Kasten T, Morris JC, Yarasheski KE, and Bateman RJ. Decreased clearance of CNS beta-amyloid in Alzheimer's disease. *Science* 330: 1774, 2010.
47. Mcmahon M, Itoh K, Yamamoto M, and Hayes JD. Keap1-dependent proteasomal degradation of transcription factor Nrf2 contributes to the negative regulation of antioxidant response element-driven gene expression. *J Biol Chem* 278: 21592–21600, 2003.
48. Meda L, Cassatella MA, Szendrei GI, Otvos L Jr, Baron P, Villalba M, Ferrari D, and Rossi F. Activation of microglial cells by beta-amyloid protein and interferon-gamma. *Nature* 374: 647–650, 1995.
49. Olagnier D, Lavergne RA, Meunier E, Lefèvre L, Dardenne C, Aubouy A, Benoit-Vical F, Ryffel B, Coste A, Berry A, and Pipy B. Nrf2, a PPARgamma alternative pathway to promote CD36 expression on inflammatory macrophages: implication for malaria. *PLoS Pathog* 7: e1002254, 2011.
50. Park L, Wang G, Zhou P, Zhou J, Pitstick R, Previti ML, Younkin L, Younkin SG, Van Nostrand WE, Cho S, Anrather J, Carlson GA, and Iadecola C. Scavenger receptor CD36 is essential for the cerebrovascular oxidative stress and neurovascular dysfunction induced by amyloid-beta. *Proc Natl Acad Sci U S A* 108: 5063–5068, 2011.
51. Patel SN, Lu Z, Ayi K, Serghides L, Gowda DC, and Kain KC. Disruption of CD36 impairs cytokine response to Plasmodium falciparum glycosylphosphatidylinositol and confers susceptibility to severe and fatal malaria *in vivo*. *J Immunol* 178: 3954–3961, 2007.
52. Peers C, Dallas ML, Boycott HE, Scragg JL, Pearson HA, and Boyle JP. Hypoxia and neurodegeneration. *Ann N Y Acad Sci* 1177: 169–177, 2009.
53. Peers C, Pearson HA, and Boyle JP. Hypoxia and Alzheimer's disease. *Essays Biochem* 43: 153–164, 2007.
54. Pialoux V, Mounier R, Brown AD, Steinback CD, Rawling JM, and Poulin MJ. Relationship between oxidative stress and HIF-1 alpha mRNA during sustained hypoxia in humans. *Free Radic Biol Med* 46: 321–326, 2009.
55. Qing H, He G, Ly PT, Fox CJ, Staufenbiel M, Cai F, Zhang Z, Wei S, Sun X, Chen CH, Zhou W, Wang K, and Song W. Valproic acid inhibits Abeta production, neuritic plaque formation, and behavioral deficits in Alzheimer's disease mouse models. *J Exp Med* 205: 2781–2789, 2008.
56. Querfurth HW and Laferla FM. Alzheimer's disease. *N Engl J Med* 362: 329–344, 2010.
57. Ramsey CP, Glass CA, Montgomery MB, Lindl KA, Ritson GP, Chia LA, Hamilton RL, Chu CT, and Jordan-Sciutto KL. Expression of Nrf2 in neurodegenerative diseases. *J Neuropathol Exp Neurol* 66: 75–85, 2007.
58. Sahin K, Tuzcu M, Gencoglu H, Dogukan A, Timurkan M, Sahin N, Aslan A, and Kucuk O. Epigallocatechin-3-gallate activates Nrf2/HO-1 signaling pathway in cisplatin-induced nephrotoxicity in rats. *Life Sci* 87: 240–245, 2010.
59. Sanchez A, Tripathy D, Yin X, Desobry K, Martinez J, Riley J, Gay D, Luo J, and Grammas P. p38 MAPK: a mediator of hypoxia-induced cerebrovascular inflammation. *J Alzheimer's Dis* 32: 587–597, 2012.
60. Schubert D, Soucek T, and Blouw B. The induction of HIF-1 reduces astrocyte activation by amyloid beta peptide. *Eur J Neurosci* 29: 1323–1334, 2009.
61. Selkoe DJ. Alzheimer's disease is a synaptic failure. *Science* 298: 789–791, 2002.
62. Semenza GL. HIF-1: mediator of physiological and pathophysiological responses to hypoxia. *J Appl Physiol (1985)* 88: 1474–1480, 2000.
63. Shao G, Gao CY, and Lu GW. Alterations of hypoxia-inducible factor-1 alpha in the hippocampus of mice acutely and repeatedly exposed to hypoxia. *Neurosignals* 14: 255–261, 2005.
64. Silverstein RL and Febbraio M. CD36, a scavenger receptor involved in immunity, metabolism, angiogenesis, and behavior. *Sci Signal* 2: re3, 2009.
65. Skoog I and Gustafson D. Update on hypertension and Alzheimer's disease. *Neurol Res* 28: 605–611, 2006.
66. Stewart CR, Stuart LM, Wilkinson K, Van Gils JM, Deng J, Halle A, Rayner KJ, Boyer L, Zhong R, Frazier WA, Lacy-Hulbert A, El Khoury J, Golenbock DT, and Moore KJ. CD36 ligands promote sterile inflammation through assembly of a Toll-like receptor 4 and 6 heterodimer. *Nat Immunol* 11: 155–161, 2010.
67. Sun X, Erb H, and Murphy TH. Coordinate regulation of glutathione metabolism in astrocytes by Nrf2. *Biochem Biophys Res Commun* 326: 371–377, 2005.
68. Sun X, He G, Qing H, Zhou W, Dobie F, Cai F, Staufenbiel M, Huang LE, and Song W. Hypoxia facilitates Alzheimer's disease pathogenesis by up-regulating BACE1 gene expression. *Proc Natl Acad Sci U S A* 103: 18727–18732, 2006.
69. Sykiotis GP, Habeos IG, Samuelson AV, and Bohmann D. The role of the antioxidant and longevity-promoting Nrf2 pathway in metabolic regulation. *Curr Opin Clin Nutr Metab Care* 14: 41–48, 2011.
70. Tabner BJ, El-Agnaf OM, Turnbull S, German MJ, Paleologou KE, Hayashi Y, Cooper LJ, Fullwood NJ, and Allsop D. Hydrogen peroxide is generated during the very early stages of aggregation of the amyloid peptides impli-

cated in Alzheimer disease and familial British dementia. *J Biol Chem* 280: 35789–35792, 2005.
71. Taylor CT. Mitochondria and cellular oxygen sensing in the HIF pathway. *Biochem J* 409: 19–26, 2008.
72. Wang CY, Xie JW, Wang T, Xu Y, Cai JH, Wang X, Zhao BL, An L, and Wang ZY. Hypoxia-triggered m-calpain activation evokes endoplasmic reticulum stress and neuropathogenesis in a transgenic mouse model of Alzheimer's disease. *CNS Neurosci Ther* 19: 820–833, 2013.
73. Wang CY, Xie JW, Xu Y, Wang T, Cai JH, Wang X, Zhao BL, An L, and Wang ZY. Trientine reduces BACE1 activity and mitigates amyloidosis via the AGE/RAGE/NF-kappaB pathway in a transgenic mouse model of Alzheimer's disease. *Antioxid Redox Signal* 19: 2024–2039, 2013.
74. Wang J, Fields J, Zhao C, Langer J, Thimmulappa RK, Kensler TW, Yamamoto M, Biswal S, and Doré S. Role of Nrf2 in protection against intracerebral hemorrhage injury in mice. *Free Radic Biol Med* 43: 408–414, 2007.
75. Wild AC, Moinova HR, and Mulcahy RT. Regulation of gamma-glutamylcysteine synthetase subunit gene expression by the transcription factor Nrf2. *J Biol Chem* 274: 33627–33636, 1999.
76. Yamanaka M, Ishikawa T, Griep A, Axt D, Kummer MP, and Heneka MT. PPARgamma/RXRalpha-induced and CD36-mediated microglial amyloid-beta phagocytosis results in cognitive improvement in amyloid precursor protein/presenilin 1 mice. *J Neurosci* 32: 17321–17331, 2012.
77. Zhang X and Le W. Pathological role of hypoxia in Alzheimer's disease. *Exp Neurol* 223: 299–303, 2010.
78. Zhang X, Li L, Zhang X, Xie W, Li L, Yang D, Heng X, Du Y, Doody RS, and Le W. Prenatal hypoxia may aggravate the cognitive impairment and Alzheimer's disease neuropathology in APPSwe/PS1A246E transgenic mice. *Neurobiol Aging* 34: 663–678, 2013.

Address correspondence to:
Prof. Zhan-You Wang
Key Laboratory of Medical Cell Biology of Ministry of Education of China
Department of Pathophysiology
China Medical University
Shenyang 110001
China

E-mail: wangzy@mail.neu.edu.cn

Prof. Li An
Department of Nutrition and Food Hygiene
School of Public Health
China Medical University
Shenyang 110001
China

E-mail: anli@mail.cmu.edu.cn

Date of first submission to ARS Central, January 10, 2014; date of final revised submission, March 31, 2014; date of acceptance, April 5, 2014.

Abbreviations Used

AD = Alzheimer's disease
ANOVA = analyses of variance
ARE = antioxidant-responsive elements
Aβ = β-amyloid
CAT = catalase
GFAP = glial fibrillary acidic protein
GSH-PX = glutathione peroxidase
HIF1α = hypoxia inducible factor 1 alpha
HO-1 = heme oxygenase-1
IDE = Insulin degradation enzyme
IL-1β = interleukin-1β
Keap1 = Kelch-like ECH associating protein 1
LV-NRF2 = a lentiviral vector encoding human NRF2
MDA = malondialdehyde
MMP-9 = matrix metalloproteinase-9
MWM = Morris water maze
NEP = neprilysin
NQO1 = nicotinamide adenine dinucleotide phosphate quinone oxidorreductase-1
NRF2 = nuclear factor erythroid 2-related factor 2
PMSF = phenylmethylsulfonyl-fluoride
ROS = reactive oxygen species
SNAP-25 = synaptosomal-associated protein 25-kDa
SYP = synaptophysin
TNFα = tumor necrosis factor-α
WT = wild-type
γGCL-C = catalytic subunits of γ-glutamyl cysteine ligase
γGCL-M = modulatory subunits of γ-glutamyl cysteine ligase